

# Heterogeneous Mean Field Game Framework for LEO Satellite-Assisted V2X Networks

Kangkang Sun, Jianhua Li, *Senior Member, IEEE*, Xiuzhen Chen, *Member, IEEE*,  
Minyi Guo, *Fellow, IEEE*

**Abstract**—Coordinating mixed fleets of huge amount of heterogeneous vehicles, passenger cars, freight trucks, and autonomous vehicles, under stringent delay constraints is a central scalability bottleneck in next-generation V2X networks. Heterogeneous mean field games (HMFG) offer a principled coordination framework, yet a fundamental design question lacks theoretical guidance: how many agent types  $K$  should be used for a fleet of size  $N$ ? The core challenge is a two-sided trade-off that existing theory does not resolve: increasing  $K$  reduces type-discretization error but simultaneously starves each class of the samples needed for reliable mean-field approximation. We resolve this trade-off by deriving an explicit  $\varepsilon$ -Nash error decomposition driven by a Wasserstein-based heterogeneity measure, and prove that the unique error-minimizing type count satisfies  $K^*(N) = \Theta(N^{1/3})$  in the canonical one-dimensional queue setting. We further establish a heterogeneity-aware convergence condition for G-prox PDHG and extend the framework to temporal-graph LEO satellite backhaul dynamics with provable robustness guarantees. A perhaps surprising consequence is that even for  $N = 10^5$  vehicles, only about 28 type classes suffice, cube-root compression rather than per-vehicle modeling, so type-granularity selection is largely a set-once design decision. Experiments validate the scaling law, achieve  $2.3\times$  faster PDHG convergence at  $K = 5$ , and deliver up to 29.5% lower delay and 60% higher throughput compared with homogeneous baselines.

**Index Terms**—Heterogeneous mean field game, V2X communications, LEO satellite networks,  $\varepsilon$ -Nash equilibrium, resource allocation.

## I. INTRODUCTION

The global proliferation of connected vehicles is reshaping the design requirements of next-generation wireless networks. By 2030, metropolitan areas are projected to support fleets of  $10^4$  to  $10^5$  heterogeneous vehicles, spanning passenger cars, freight trucks, and autonomous vehicles, each generating continuous sensor traffic that must be offloaded to multi-access edge computing (MEC) servers under strict latency constraints [1], [2]. In large-scale vehicle-to-everything (V2X) systems, the core resource-allocation question is not only how to allocate power and computation, but whether the underlying game model faithfully represents the population it coordinates.

When  $N$  vehicles interact directly, coordination complexity grows as  $O(N^2)$ , making exact Nash computation intractable

Kangkang Sun, Jianhua Li, Xiuzhen Chen and Minyi Guo are with the Shanghai Key Laboratory of Integrated Administration Technologies for Information Security, School of Computer Science, Shanghai Jiao Tong University, Shanghai 200240, China (e-mail: szpsunkk@sjtu.edu.cn; lijh888@sjtu.edu.cn; xzchen@sjtu.edu.cn; guo-my@cs.sjtu.edu.cn).

*Corresponding author: Jianhua Li.*

This work has been submitted to the IEEE for possible publication. Copyright may be transferred without notice, after which this version may no longer be accessible.

for even moderate fleet sizes. Mean field game (MFG) theory [1], [2] resolves this by replacing the aggregate influence of all other vehicles with a population-level distribution, reducing per-iteration complexity to  $O(1)$  in vehicle count. Building on this, Kang et al. [3] developed a G-prox Primal-Dual Hybrid Gradient (PDHG) solver for automotive MEC offloading with vehicle-count-independent behavior, and Wang et al. [4] extended MFG to LEO-assisted offloading. These works demonstrate that MFG is practically viable for large-scale V2X coordination.

Homogeneous MFG treats all vehicles as statistically identical, which is unrealistic for mixed fleets. Autonomous vehicles may generate substantially higher sensor loads than passenger cars, while freight vehicles operate under distinct energy and delay constraints. Ignoring such heterogeneity inflates the  $\varepsilon$ -Nash approximation error and degrades fairness and throughput across classes. Heterogeneous MFG (HMFG) addresses this by partitioning the fleet into  $K$  agent types [5]–[7]. Empirical studies report significant gains from type-aware control, confirming the practical value of heterogeneity modeling.

Despite this progress, one key question remains unresolved: *for a fleet of  $N$  vehicles, how many types  $K$  should be distinguished?* Existing HMFG/MARL works often fix  $K$  heuristically [5], [6], while the well-posedness analysis in [7] does not provide an error-minimizing selection rule. The difficulty comes from two opposing effects. Increasing  $K$  decreases type-discretization error because finer bins better represent population diversity. At the same time, increasing  $K$  reduces per-class sample size  $N_k \approx N/K$ , weakening the finite-sample accuracy of the mean-field approximation and increasing sampling error. The balance yields a nontrivial optimal  $K^*(N)$  not determined by classical quantization theory [8] or graphon MFG [9], [10] alone. The challenge is sharpened in LEO-assisted V2X. Fast satellite topology changes introduce non-stationary backhaul surcharges in HMFG dynamics, potentially affecting the stability and robustness of iterative equilibrium solvers designed under static assumptions [4], [11].

A rigorous framework is established for optimal type granularity in HMFG-based V2X networks with LEO-assisted backhaul. The interplay among type granularity, solver stability, and network dynamics gives rise to three closely related questions whose answers determine whether HMFG can be deployed at scale:

- **Q1 (Granularity):** *For a fleet of  $N$  vehicles, what is the optimal type count  $K^*(N)$ , and how does it scale with  $N$ ?*

- **Q2 (Convergence):** How should PDHG step sizes adapt to heterogeneity to guarantee stable and fast convergence?
- **Q3 (Robustness):** Does the optimal granularity law remain valid under time-varying LEO topology?

The answers are concise and actionable: Q1 yields  $K^*(N) = \Theta(N^{1/3})$ , Q2 yields a heterogeneity-dependent step-size shrinkage rule, and Q3 is affirmative under a mild topology-variation condition, summarized next as three technical contributions.

- *Optimal type-count law.* The  $\varepsilon$ -Nash error via a Wasserstein-based heterogeneity measure is decomposed (Theorem 1), and the unique minimizer  $K^*(N) = \Theta(N^{1/3})$  in the 1D queue setting is derived (Theorem 2). **Key insight:** even a  $10^5$ -vehicle fleet needs only about 28 types.
- *Heterogeneity-aware convergence.* A sufficient multi-type PDHG step-size condition is derived (Theorem 4) and an adaptive rule that yields  $2.3\times$  faster convergence than an aggressive fixed-step baseline at  $K = 5$ .
- *LEO-robust scalable framework.* Temporal-graph LEO backhaul dynamics are embedded, and cube-root scaling is shown to remain order-optimal under bounded topology variation (Theorem 3). The resulting three-algorithm pipeline achieves up to 29.5% lower delay and 60% higher throughput than homogeneous baselines.

Relative to [3], the proposed framework reduces to the homogeneous case at  $K = 1$ , and the convergence condition recovers the classical criterion when  $H_K = 0$ . Relative to [5], [6], a principled type-count selection rule is provided in place of a fixed heuristic choice of  $K$ . Relative to [7], the practical decomposition needed to derive explicit  $K^*$  to  $N$  scaling is sharpened. Relative to [11], temporal-graph LEO dynamics are embedded directly into HMFG and robustness guarantees are established. Relative to [12], the analytical HMFG guarantees complement optimization-driven learning in uncertain and non-stationary regimes.

The remainder of the paper is organized as follows. Section II reviews related work. Section III presents the V2X system model and HMFG formulation. Section IV introduces the heterogeneity measure and error decomposition. Section V derives the optimal granularity scaling law. Section VI develops the three-algorithm framework with convergence analysis. Section VII presents numerical evaluation. Section VIII provides practical guidelines. Section IX concludes.

*Notation.*  $\mathcal{P}(E)$  denotes the space of Borel probability measures on a Polish space  $E$ .  $W_p(\mu, \nu)$  is the Wasserstein- $p$  distance.  $\|\cdot\|_{L^2}$  and  $\|\cdot\|_{H^1}$  are standard Sobolev norms. For  $n \in \mathbb{N}$ ,  $[n] := \{1, \dots, n\}$ .  $\mathbb{1}_A$  is the indicator of event  $A$ . Bold symbols  $\boldsymbol{\rho} = (\rho^{(1)}, \dots, \rho^{(K)})$  denote  $K$ -tuples;  $\|\mathbf{A}\|_{\text{op}}$  is the operator norm.

## II. RELATED WORK

We organize prior work into four strands: scalable MFG applications and solvers in wireless and vehicular systems (Section II-A); HMFG theory, propagation of chaos, and empirical measure convergence rates (Section II-B); models of heterogeneity including quantization theory and graphon limits (Section II-C); and related optimization and learning approaches for dynamic spectrum and resource allocation (Section II-D).

### A. MFG Applications and Primal-Dual Solvers in Wireless and V2X

Mean field game theory [1], [2] has become a leading framework for scalable resource management in large vehicular and wireless networks. Its Hamilton-Jacobi-Bellman and Fokker-Planck-Kolmogorov structure decouples each agent from pairwise interactions, allowing equilibrium computation in time that does not grow with fleet size.

For automotive multi-access edge computing, Kang et al. [3] showed that a G-prox Primal-Dual Hybrid Gradient solver achieves exactly this vehicle-count independence. Their work builds on the Chambolle-Pock primal-dual framework [13], and our convergence theorem in Section VI extends their homogeneous step-size criterion to the multi-type setting via the heterogeneity measure. Wang et al. [4], [14] applied Stackelberg MFG to distributed offloading in ultra-dense LEO satellite networks. Wang et al. [15] extended MFG control to integrated sensing, communication, and computation waveform precoding. Kang et al. [16] used mean-field evolutionary dynamics for satellite-based federated learning.

Motivated by the diversity of real-world fleets, several lines of work adopt multi-type learning approaches. Zhang et al. [5] proposed a two-type heterogeneous mean-field multi-agent reinforcement learning scheme for space-air-ground integrated networks, reporting approximately eighty percent throughput gains. Xu et al. [6] developed a multi-type mean-field MARL scheme for joint power and offloading control in V2X. Shen and Huang [17] addressed heterogeneous IoT devices in RIS-assisted satellite-aerial-ground networks. A survey by Jiang et al. [18] covers game-theoretic approaches to satellite communication networks more broadly. Across all these works, the number of agent types is fixed by design, often at two, without a quantitative rule linking the type count to fleet size or to sampling accuracy. Resolving this gap is the primary contribution of the present paper.

### B. HMFG Well-Posedness, Propagation of Chaos, and Empirical Convergence Rates

The local well-posedness of multi-population heterogeneous mean field games and the associated equilibrium approximation bound are due to Qiao [7]. This work establishes that the approximation error depends on three terms: a type-discretization component, an initial-condition mismatch component, and a per-class population component governed by the smallest class size. Carmona and Delarue [19] provide the broader probabilistic MFG apparatus, including propagation-of-chaos estimates for finite-population empirical laws.

These foundational results justify HMFG for a fixed number of types but do not decompose the error into discretization and sampling components, and they offer no guidance for optimizing the type count. Our Theorem 1 fills this gap by making the decomposition explicit, using the sharp one-dimensional Wasserstein empirical convergence rate established by Fournier and Guillin [20]. This rate, which scales as the square root of inverse sample size in one dimension, is stronger than the generic rate available in higher dimensions and is the

key ingredient that allows us to derive the cube-root scaling law for the optimal type count.

We note that our derivation reconciles with the bound of [7]: in the regime where the type count grows as the cube root of fleet size, the per-class population term in [7] is strictly dominated by our sampling term, so our bound is not looser. Remark 8.5(ii) of [7] itself notes that propagation-of-chaos rates can be sharpened through improved empirical measure estimates; we adopt the sharp one-dimensional rate throughout. In summary, propagation-of-chaos theory and HMFG well-posedness justify finite type modeling but do not answer how many types to use; our error decomposition closes this gap and leads directly to the cube-root scaling law.

### C. Quantization Theory, Graphon Limits, and Finite Type versus Continuum Models

Finite-type design in mean-field games is formally analogous to vector quantization [8]. In classical source coding, type representatives form a codebook, and the distortion from representing a continuum of types by a finite codebook decreases as a Hölder power of the codebook size. This is precisely the discretization component in our error decomposition. However, mean-field validity imposes an additional constraint that has no counterpart in classical source coding: each type class must contain enough agents for the law-of-large-numbers argument to hold. This sampling constraint produces the opposing term in our decomposition, a term that increases rather than decreases as more types are added, and it is the interaction between these two terms that yields a finite optimal type count.

An alternative formulation uses a continuum of agent types, as in graphon mean-field games [9], [10]. In these models, each agent carries a continuous type label and the population is described by a measure over the type space. This continuum formulation is elegant and mathematically natural, but it has no direct analog of the finite-sample constraint that arises when each type class contains only finitely many vehicles. Our finite-type HMFG can be read as a rate-distortion approximation to such continuum models, and taking the fleet size to infinity first recovers the continuum limit with an optimal type count that grows without bound. Weed and Bach [21] sharpen empirical Wasserstein rates under low intrinsic dimension, consistent with our one-dimensional analysis. Type-aggregation and graph-topology models in [19] emphasize latent structure rather than the ordered capability heterogeneity that characterizes real V2X deployments; our setting is tailored to this ordered structure. Neither classical quantization nor graphon MFG captures the interaction between discretization fidelity and finite-sample reliability in practical HMFG deployment; our framework bridges this gap with an explicit sampling-constrained rate-distortion view and a closed-form  $N$ -scaling law.

### D. Optimization-Driven Learning and LEO-Assisted Communication

Optimization-driven deep reinforcement learning provides a complementary perspective for resource allocation in dynamic wireless environments. Ding et al. [12] proposed an optimization-driven DRL framework for joint resource

allocation and trajectory optimization in UAV spectrum sharing networks under uncertain jamming. The key innovation is to derive model-based lower bounds on the worst-case sum rate and inject them as informed target values into the DRL training process. This integration of model-based structure into data-driven learning improves convergence speed by approximately two hundred training episodes compared to pure DRL and helps the agent escape local optima in the early training phase. Our HMFG approach takes the complementary direction: rather than accelerating data-driven learning with model-based bounds, we exploit the full analytical structure of the HJB-FPK system to obtain provable equilibrium guarantees with per-iteration complexity independent of vehicle count. The two paradigms are well-suited to different operating conditions. When the channel and interference model are known and stationary, our analytical approach delivers verifiable bounds; when these conditions are uncertain or non-stationary, optimization-driven DRL offers adaptive robustness.

For LEO satellite-assisted networks, Guo et al. [11] developed a semantic communication-compliant shortest path selection framework for large-scale Starlink-based constellations. Their central contribution is a temporal-graph model of satellite topology: the network is represented as a sequence of approximately stable snapshot graphs, each valid for a time window of roughly sixty seconds, and path selection is solved optimally within each snapshot using properties of Dijkstra's algorithm. The framework shows that semantic compression, which reduces transmitted data volume by a factor of two to eight, can substantially reduce occupied bandwidth at the cost of slightly increased delay, and that this trade-off improves as the fraction of semantics-capable satellites increases. Our work borrows the temporal-graph snapshot model from [11] and embeds it into the HMFG cost function as a time-varying backhaul surcharge. We prove that the optimal type-count scaling law remains order-optimal under this perturbation provided per-snapshot bandwidth variation satisfies a mild decay condition with fleet size. The two works are synergistic: semantic compression at the vehicle-satellite interface reduces effective traffic load, which lowers the heterogeneity measure and therefore permits a smaller optimal type count in our framework. Joint optimization of semantic compression ratio and type granularity is identified as a promising direction for future work; in summary, neither optimization-driven DRL nor semantic-aware LEO path selection addresses HMFG type-granularity design, and the present framework fills this gap with explicit scaling laws that remain order-optimal under LEO topology variation.

## III. SYSTEM MODEL AND HMFG FORMULATION

This section builds the HMFG-V2X model in four steps: mixed-fleet scenario and type partition, queue and transmission dynamics, type-dependent cost with LEO backhaul effects, and the coupled HJB-FPK equilibrium system. The key modeling choice is class-specific cost weighting  $\{\beta_1^{(k)}, \beta_2^{(k)}, C^{(k)}\}$ , which distinguishes HMFG from homogeneous MFG and directly drives the type-granularity trade-off analyzed in Sections IV to V.

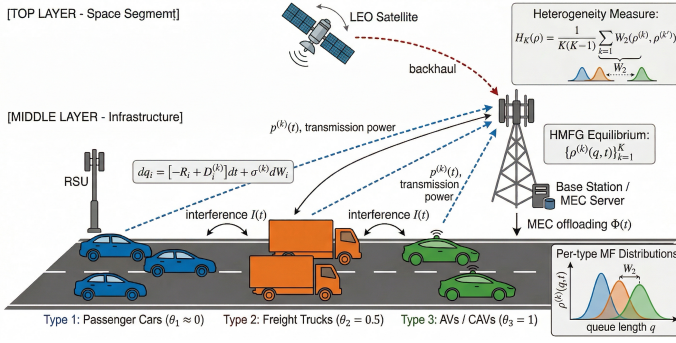


Fig. 1. Illustrative V2X-MEC scenario for heterogeneous mean field resource allocation. The diverse vehicle population is partitioned into  $K$  types with distinct data loads and preferences. Per-type mean fields  $\rho^{(k)}$  capture class-wise congestion, while cross-type coupling enters through interference  $I(t)$  and the computational price  $\Phi(t)$ .

### A. Scenario Description

As illustrated in Fig. 1, we consider a V2X communication network where a roadside infrastructure node (RSU) equipped with multi-access edge computing (MEC) serves a large mixed fleet of  $N$  vehicles. The vehicles are heterogeneous in terms of data generation rates, energy constraints, and QoS requirements, which motivates a  $K$ -type partition framework for HMFG-based resource allocation.

Let  $\mathcal{N} = \{1, \dots, N\}$  denote the vehicle set, which is partitioned into  $K$  disjoint types:

$$\mathcal{N} = \bigsqcup_{k=1}^K \mathcal{C}_k, \quad |\mathcal{C}_k| = N_k, \quad \sum_{k=1}^K N_k = N, \quad (1)$$

where type  $k \in [K]$  represents a distinct vehicle class. For example, in a three-class model:  $k = 1$  for passenger cars,  $k = 2$  for freight trucks, and  $k = 3$  for autonomous vehicles. The heterogeneity across types manifests in three dimensions:

- *State dynamics*: Data generation rates  $D_i^{(k)}(t)$  differ across vehicle classes, with autonomous vehicles generating significantly more sensor data than passenger cars.
- *Cost preferences*: Energy-vs.-delay trade-off weights  $\beta_1^{(k)}, \beta_2^{(k)}$  encode class-specific priorities.
- *Action constraints*: Maximum transmission power and computational budgets reflect hardware differences among vehicle types.

### B. Data Queue Dynamics

The state of vehicle  $i \in \mathcal{C}_k$  is characterized by its data queue length  $q_i(t) \in \Omega = [0, Q_{\max}]$ . The queue dynamics follow the stochastic differential equation:

$$dq_i(t) = \underbrace{\left[ -R_i(t) + D_i^{(k)}(t) \right]}_{\text{drift}} dt + \underbrace{\sigma^{(k)} dW_i(t)}_{\text{diffusion}}, \quad (2)$$

where  $R_i(t)$  is the transmission rate,  $D_i^{(k)}(t)$  is the type- $k$  dependent data generation rate,  $\sigma^{(k)} > 0$  is the diffusion coefficient capturing queue uncertainty, and  $\{W_i(t)\}$  are

independent standard Brownian motions. The transmission rate under the SINR model [15] is given by:

$$R_i(t) = B \log_2 \left( 1 + \frac{p_i(t)g_i(t)}{\sigma_c^2 + I(t)} \right), \quad (3)$$

where  $B$  is the channel bandwidth,  $p_i(t) \in [0, P_{\max}]$  is the transmission power,  $g_i(t)$  is the channel gain,  $\sigma_c^2$  is the noise variance, and  $I(t) = \sum_{j \neq i} p_j(t)g_j(t)$  is the aggregate interference.

### C. Cost Function Formulation

Each vehicle  $i$  of type  $k$  minimizes the expected cumulative cost over the time horizon  $[0, T]$ :

$$J_i^{(k)}(p_i) = \mathbb{E} \left[ \int_0^T \left( \beta_1^{(k)} p_i^2(t) + \beta_2^{(k)} \Phi(t) R_i(t) \right) dt + C^{(k)} q_i(T)^2 \right], \quad (4)$$

where  $\beta_1^{(k)}, \beta_2^{(k)} > 0$  are type-dependent energy and offloading weights,  $C^{(k)}$  is the terminal queue penalty, and

$$\Phi(t) = \kappa + \rho \int_{\Omega} R(q, t) \rho(q, t) dq + \frac{\mu}{B_{\text{sat}}^{\tau(t)}}, \quad (5)$$

is the congestion-aware computational price with LEO backhaul correction, where  $B_{\text{sat}}^{\tau(t)}$  is the available satellite backhaul bandwidth in the active snapshot  $\tau(t)$  and  $\mu > 0$  is the backhaul-cost coefficient. The heterogeneous cost weights  $\{\beta_1^{(k)}, \beta_2^{(k)}, C^{(k)}\}$  constitute the primary source of agent heterogeneity in our HMFG formulation.

### D. LEO Satellite-Assisted Backhaul Model

Following the temporal-graph view in [11], we represent the LEO constellation by snapshots  $\mathcal{G}^{\tau} = (\mathcal{V}^{\tau}, \mathcal{L}^{\tau})$  that remain approximately stable over each time window  $\tau$ . The effective RSU-MEC backhaul bandwidth through the current satellite route is modeled as

$$B_{\text{sat}}^{\tau} = \min_{(O_i, O_j) \in \mathcal{L}^{\tau}} r_{O_i, O_j}^{\tau}, \quad (6)$$

where  $r_{O_i, O_j}^{\tau}$  denotes the per-link capacity on the selected path. This model captures the fact that fast topology changes perturb the backhaul term in (5), thereby affecting both the HJB cost and FPK drift through coupled congestion dynamics. Following the Starlink-oriented setting in [11], we use  $r_{O_i, O_j}^{\tau} \sim \mathcal{U}[300, 350]$  Mbps and  $\Delta\tau = 60$  s in simulations, which yields a bounded snapshot perturbation  $\Delta_{\Phi}$  in (28) for realistic  $\mu \leq 1$ .

### E. Heterogeneous Mean Field Game Formulation

Following the HMFG framework of [7], as  $N \rightarrow \infty$  with  $K$  fixed, the finite-player game converges to a  $K$ -population MFG characterized by the per-type mean field densities  $\rho = \{\rho^{(k)}(q, t)\}_{k=1}^K$ . The HMFG equilibrium is defined by the coupled Hamilton-Jacobi-Bellman (HJB) and Fokker-Planck-Kolmogorov (FPK) system:

**HJB equations** (backward in time, for each  $k \in [K]$ ):

$$-\frac{\partial V^{(k)}}{\partial t} + \mathcal{H}^{(k)} \left( q, \rho, \frac{\partial V^{(k)}}{\partial q} \right) = 0, \quad (7)$$

with terminal condition  $V^{(k)}(q, T) = C^{(k)}q^2$ .

**FPK equations** (forward in time, for each  $k \in [K]$ ):

$$\frac{\partial \rho^{(k)}}{\partial t} + \frac{\partial}{\partial q} \left( \rho^{(k)} \cdot \Gamma^{(k)}[q, t, \rho] \right) = \frac{(\sigma^{(k)})^2}{2} \frac{\partial^2 \rho^{(k)}}{\partial q^2}, \quad (8)$$

with initial condition  $\rho^{(k)}(q, 0) = \rho_0^{(k)}$ , where  $\Gamma^{(k)} = -R^{(k)}(q, t, \rho) + D^{(k)}(t)$  is the optimal drift and  $\mathcal{H}^{(k)}$  is the type- $k$  Hamiltonian.

**Cross-type coupling.** The coupling between types occurs through the aggregate interference:

$$I(t) = \sum_{k'=1}^K N_{k'} \int_{\Omega} p^{(k')}(q, t) |h^{(k')}(t)|^2 \rho^{(k')}(q, t) dq + I_{\text{sat}}^{\tau}(t), \quad (9)$$

where  $I_{\text{sat}}^{\tau}(t) \in [0, \bar{I}_{\text{sat}}]$  models residual LEO downlink interference in snapshot  $\tau$ . Together with computational price  $\Phi(t)$  in (5), both terms depend on all  $K$  mean field distributions, creating the heterogeneous coupling that distinguishes HMFG from the homogeneous case.

**Remark 1** (Reduction to Homogeneous MFG). *When  $K = 1$  and all vehicles are identical, system (7) to (8) reduces to the standard homogeneous MFG of [3], for which G-prox PDHG converges with complexity  $O(N_q \times N_t)$ , independent of  $N$ .*

#### F. Problem Formulation

The central problem addressed in this paper is the joint optimization of:

- 1) **Type granularity selection:** Determine the optimal number of types  $K^*(N)$  given fleet size  $N$ .
- 2) **HMFG equilibrium computation:** Solve the coupled HJB-FPK system (7) to (8) efficiently with convergence guarantees under heterogeneous coupling.
- 3) **Resource allocation:** Compute the optimal power allocation policy  $\{p^{(k)*}(q, t)\}_{k=1}^K$  that minimizes the aggregate cost across all vehicle types.

The fundamental challenge is the *type-granularity trade-off*: increasing  $K$  captures more heterogeneity but reduces per-class sample size, degrading the mean-field approximation accuracy. Our framework provides a principled resolution to this trade-off through explicit error decomposition and optimal  $K^*$  characterization. The next section formalizes this trade-off by quantifying heterogeneity and decomposing the  $\varepsilon$ -Nash error into discretization and sampling terms.

## IV. HETEROGENEITY MEASURE AND ERROR DECOMPOSITION

### A. Quantifying Heterogeneity

A central contribution of this paper is a formal measure of the ‘‘distance from homogeneity’’ for a  $K$ -type partition  $\{C_k\}_{k=1}^K$  with associated state distributions  $\{\rho^{(k)}\}_{k=1}^K$ .

**Definition 1** (Heterogeneity Measure). *For a  $K$ -type HMFG with per-type initial distributions  $\rho_0^{(k)} \in \mathcal{P}(\Omega)$ , the heterogeneity measure is:*

$$H_K(\rho_0) := \frac{1}{K(K-1)} \sum_{k \neq k'} W_2(\rho_0^{(k)}, \rho_0^{(k')}), \quad (10)$$

where  $W_2(\mu, \nu) = \inf_{\pi \in \Gamma(\mu, \nu)} (\mathbb{E}_{\pi} |X - Y|^2)^{1/2}$  is the Wasserstein-2 distance, and  $\Gamma(\mu, \nu)$  is the set of couplings.

**Remark 2.** *The measure  $H_K(\rho_0)$  equals zero if and only if all  $K$  types have identical initial distributions, i.e., the system is effectively homogeneous. As  $K \rightarrow \infty$  with a fixed continuum of types,  $H_K(\rho_0)$  converges to the average pairwise Wasserstein distance in the type space  $[0, 1]$ :*

$$H_{\infty}(\rho_0) = \int_0^1 \int_0^1 W_2(\rho_0^{\alpha}, \rho_0^{\beta}) d\alpha d\beta, \quad (11)$$

where  $\rho_0^{\alpha}$  is the distribution of the type- $\alpha$  player in the continuum HMFG of [7].

### B. Parameterized Heterogeneous Model

To enable concrete analysis, we consider the following parameterized model, which is general enough to capture the essential structure while admitting closed-form calculations.

**Assumption 1** (Parameterized Heterogeneity). *The type- $k$  drift coefficient takes the form:*

$$b^{(k)}(q, \rho, a) = b_0(q, \rho, a) + \theta_k \cdot b_1(q, \rho, a), \quad (12)$$

where  $b_0, b_1 : \Omega \times \mathcal{M} \times A \rightarrow \mathbb{R}$  are fixed functions (common to all types) and  $\theta_k \in [0, 1]$  is the type parameter characterizing the deviation of type  $k$  from the baseline ( $\theta_k = 0$ ). The parameters are ordered:  $0 = \theta_1 < \theta_2 < \dots < \theta_K = 1$ .

This parameterization is motivated by the empirical observation that vehicle-class capabilities, data rate, power budget, and delay tolerance, can be ordered along a single capability axis in practical V2X deployments [5], [6]. The linear-in- $\theta$  form captures ordered heterogeneity while admitting closed-form error bounds; nonlinear  $\theta$ -dependence mainly changes  $\beta$  but not the scaling-law structure (see Remark 8).

Under Assumption 1, the heterogeneity measure (10) can be related to the variance of the type parameters:

**Lemma 1** (Heterogeneity Measure under Parameterization). *Under Assumption 1, suppose  $b_1$  is  $L_b$ -Lipschitz in  $(q, \rho)$  uniformly over  $a \in A$ . Then:*

$$H_K(\rho_0) \leq L_b T \cdot \text{Var}(\theta)^{1/2} + H_K^{(0)}, \quad (13)$$

where  $\text{Var}(\theta) = \frac{1}{K} \sum_k (\theta_k - \bar{\theta})^2$  is the empirical variance of type parameters,  $\bar{\theta} = \frac{1}{K} \sum_k \theta_k$ , and  $H_K^{(0)} = \frac{1}{K(K-1)} \sum_{k \neq k'} W_2(\rho_0^{(k)}, \rho_0^{(k')})$  is the initial heterogeneity.

*Proof.* See Appendix A.  $\square$

### C. Error Decomposition

We now provide the main error decomposition theorem, extending the bound

$$\varepsilon_{N,K} \leq C \left( \rho_K + \delta_{N,K} + \frac{1}{K \cdot n_{N,K}^3} \right)^{1/2}, \quad (14)$$

from [7], where  $\rho_K$  denotes type-discretization error,  $\delta_{N,K}$  denotes initial mismatch, and  $n_{N,K}$  is the smallest class population. We make the dependence on heterogeneity explicit.

**Lemma 2** (Empirical Wasserstein Rates on a Bounded Interval). *Let  $\Omega = [0, Q_{\max}]$ ,  $\mu \in \mathcal{P}(\Omega)$ , and let  $X_1, \dots, X_n$  be i.i.d. with law  $\mu$ . Define the empirical measure  $\mu_n = \frac{1}{n} \sum_{i=1}^n \delta_{X_i}$ . Then:*

- (i)  $\mathbb{E}[W_1(\mu_n, \mu)] \leq C_1^{\text{emp}} n^{-1/2}$  for a constant  $C_1^{\text{emp}}$  depending only on  $Q_{\max}$  (Theorem 1 of [20],  $d = 1$ , compact support).
- (ii)  $\mathbb{E}[W_2(\mu_n, \mu)] \leq C_2^{\text{emp}} n^{-1/2}$  for  $C_2^{\text{emp}}$  depending only on  $Q_{\max}$  (same reference; in dimension one,  $W_2$  admits the same  $n^{-1/2}$  order as  $W_1$  under the stated compactness).
- (iii) No integrability conditions beyond  $\text{supp}(\mu) \subseteq \Omega$  are needed; all moments are bounded by  $Q_{\max}$ .

*Proof.* See Appendix B.  $\square$

**Remark 3** (Reconciliation with [7]). *The bound in [7] contains the term  $\frac{1}{K \cdot n_{N,K}^3}$  with  $n_{N,K} = \min_{\ell} |C_{\ell}|$ . For balanced partitions,  $N_k \approx N/K$ , so*

$$\frac{1}{K(N/K)^3} = \frac{K^2}{N^3}. \quad (15)$$

We show this is dominated by  $(K/N)^{1/2}$  whenever  $K \leq N^{1/2}$ . Setting  $r = K/N \in (0, 1]$ , the ratio of the two terms is

$$\frac{K^2/N^3}{(K/N)^{1/2}} = \frac{K^2}{N^3} \cdot \left(\frac{N}{K}\right)^{1/2} = \frac{K^{3/2}}{N^{5/2}} = r^{3/2} N^{-1} \leq N^{-1} \rightarrow 0. \quad (16)$$

Hence for any  $K = o(N)$ , the Qiao term  $K^2/N^3$  is strictly smaller than our per-class term  $C_2(K/N)^{1/2}$  for all  $N$  sufficiently large. In the regime  $K \leq \sqrt{N}$  (which is satisfied at  $K^*(N) = \Theta(N^{1/3})$  for all  $N \geq 1$ ), (16) gives  $K^2/N^3 \leq (K/N)^{1/2}/N \leq (K/N)^{1/2}$ . Thus our per-class term  $(K/N)^{1/2}$  is not looser than the corresponding term in [7] in this regime. More broadly, Remark 8.5(ii) of [7] notes that propagation-of-chaos rates can be sharpened via improved empirical measure estimates; we adopt the sharp ID rate  $\alpha = 1/2$  from [20] throughout.

**Theorem 1** (Error Decomposition). *Under the local well-posedness assumptions of [7], namely: (A1) Lipschitz continuity of the drifts in the state and mean-field arguments; (A2) bounded, nondegenerate diffusion coefficients; and (A3) compact state space  $\Omega$ ; together with Assumption 1, the  $\varepsilon$ -Nash approximation error satisfies:*

$$\varepsilon_{N,K} \leq C_1 \cdot \underbrace{K^{-\beta}}_{\text{discretization}} + C_2 \cdot \underbrace{\left(\frac{K}{N}\right)^{\alpha}}_{\text{sample size}} + C_3 \cdot \delta_{N,K}^{1/2}, \quad (17)$$

where  $\beta > 0$  is the Hölder exponent of the drift in the type parameter (Step 1 below),  $\alpha > 0$  is the sharp rate for empirical approximation in Wasserstein distance on the state space  $\Omega$  (for  $d=1$ , we take  $\alpha = 1/2$ ; see [20]), and  $C_1, C_2, C_3 > 0$  depend on  $L, T$  and moment bounds but not on  $N, K$ .

*Proof.* See Appendix C.  $\square$

**Remark 4.** *Under Assumption 1 with  $\theta_k \in [0, 1]$ , one may also bound  $[b_1]_{\beta}$  in terms of moments of  $\theta$ , which recovers a  $\text{Var}(\theta)$  dependence at the level of constants; (17) absorbs this into  $C_1$ .*

TABLE I  
DEPENDENCIES OF KEY CONSTANTS

Constant	Depends on	Independent of
$C_1$	$L_b, T, [b_1]_{\beta}, \beta$	$N, K$
$C_2$	$Q_{\max}$	$N, K, T$
$C_3$	$L, T$	$N, K$
$C_H$	$L, T, K, \ \nabla_q \phi\ _{L^\infty}$	$N$
$L_A$	$N_q, N_t, Q_{\max}, T$	$N, K$

**Remark 5.** *Theorem 1 makes explicit the fundamental tension:*

- The term  $C_1 K^{-\beta}$  decreases with  $K$  (finer type bins).
- The term  $C_2 (K/N)^{\alpha}$  increases with  $K$  (fewer vehicles per class).

*This tension yields a finite optimal granularity  $K^*(N)$  in the reduced model.*

**Remark 6** (Summary of Constant Dependencies). *Table I summarizes the dependence of the key constants in (17) and (36) on the system parameters. The constants  $C_1, C_2$ , and  $C_3$  are independent of  $N$  and  $K$ , so the  $N$ - and  $K$ -scaling of the error bound is carried by the explicit terms  $K^{-\beta}$  and  $(K/N)^{\alpha}$ .*

The decomposition above confirms a nontrivial optimum in type granularity. The next section derives its explicit form and fleet-size scaling law.

## V. OPTIMAL HETEROGENEITY GRANULARITY

### A. Existence and Characterization of $K^*(N)$

**Theorem 2** (Existence of Optimal Granularity). *Consider the  $\varepsilon$ -Nash error (17) with constants  $C_1, C_2 > 0$ , exponents  $\alpha, \beta > 0$  as in Theorem 1, and  $\delta_{N,K}$  negligible (good initial condition matching). Define the reduced error:*

$$\mathcal{E}(N, K) := C_1 K^{-\beta} + C_2 \left(\frac{K}{N}\right)^{\alpha}. \quad (18)$$

*Then:*

- 1) For any fixed  $N$ ,  $\mathcal{E}(N, \cdot)$  attains a unique global minimum on  $(0, \infty)$  at

$$K^*(N) = \left(\frac{\beta C_1}{\alpha C_2}\right)^{1/(\alpha+\beta)} \cdot N^{\alpha/(\alpha+\beta)}. \quad (19)$$

- 2)  $K^*(N) = \Theta(N^{\gamma})$  with  $\gamma = \frac{\alpha}{\alpha+\beta} \in (0, 1)$ .
- 3) The minimum error satisfies:

$$\mathcal{E}(N, K^*(N)) = \Theta\left(N^{-\alpha\beta/(\alpha+\beta)}\right). \quad (20)$$

*Proof.* See Appendix D.  $\square$

**Corollary 1** (Practical Scaling Law). *For the 1D queue state space ( $d = 1$ ), take the sharp sample exponent  $\alpha = 1/2$  as in Lemma 2(ii) [20], and Lipschitz type dependence ( $\beta = 1$ ) in (12). Then  $\gamma = \alpha/(\alpha + \beta) = 1/3$  and*

$$K^*(N) = \Theta\left(N^{1/3}\right). \quad (21)$$

*For example,  $N^{1/3} = 10$  at  $N = 10^3$ ; absolute levels of  $K^*$  depend on the ratio  $C_1/C_2$  in (19).*

**Remark 7** (Intuition Behind the Cube-Root Law). *The cube-root exponent follows from balancing two opposing effects: discretization improves roughly as  $K^{-1}$ , while sampling reliability degrades as  $(K/N)^{1/2}$  in the 1D setting. Matching marginal gains and losses yields the characteristic  $K \sim N^{1/3}$  scaling. Practical implication: growth is slow, so type-granularity is typically a set-once, adjust-rarely design choice.*

**Remark 8** (Physical Interpretation of  $\beta$  in V2X). *In (4), heterogeneity enters the drift via class-dependent pricing and rate sensitivity. Under the SINR model (3) with LoS-dominated channels,  $b_1(q, \rho, a) = \beta_2^{(k)} \Phi(t) \cdot \partial R / \partial p$  is Lipschitz in the type parameter with constant order  $L_b = P_{\max} B / (\sigma_c^2 \ln 2)$ , so  $\beta = 1$  is well justified and leads to  $K^*(N) = \Theta(N^{1/3})$  in Corollary 1. In harsher non-LoS environments with stronger small-scale fading and abrupt channel-state transitions [12], the effective regularity may degrade to  $\beta < 1$ , which increases the recommended growth of type granularity with  $N$  and is consistent with the higher uncertainty regime usually handled by optimization-driven DRL.*

**Remark 9.** *The exponent 1/3 reflects the corrected 1D empirical rate; small integer choices  $K \in \{2, 3\}$  in [5], [6] remain compatible with (19) when effective constants imply a modest  $K^*(N)$  at moderate  $N$ .*

**Remark 10** (Higher-Dimensional State Spaces). *For a  $d$ -dimensional state (e.g., joint queue-channel  $(q_i, g_i) \in \mathbb{R}^2$ ), Fournier and Guillin [20] give  $\alpha = 1/(d+2)$  for  $d \geq 3$ , with logarithmic corrections for  $d = 2$ . With Lipschitz type dependence ( $\beta = 1$ ), Theorem 2 yields*

$$\gamma = \frac{\alpha}{\alpha + \beta} = \frac{1/(d+2)}{1/(d+2) + 1} = \frac{1}{d+3} \quad (d \geq 3),$$

whereas for  $d = 2$  one obtains  $\gamma$  of order roughly 1/4. Thus richer state descriptions slow per-class empirical convergence and imply smaller  $\gamma$ , meaning fewer types per unit  $N$  than in the 1D queue model. For measures with low intrinsic dimension  $d^* < d$ , Weed and Bach [21] give rates suggesting  $\alpha$  can improve toward  $1/d^*$ , partially recovering the sharp 1D scaling when trajectories concentrate near a low-dimensional manifold.

### B. Relationship Between $K^*(N)$ and Heterogeneity Measure

**Proposition 1** (Heterogeneity-Adjusted Optimal Granularity). *When the discretization error constant is proportional to the heterogeneity measure:  $C_1 = \bar{C}_1 \cdot H_\infty(\rho_0)$ , the optimal granularity satisfies:*

$$K^*(N; H_\infty) = \left( \frac{\beta \bar{C}_1 H_\infty}{\alpha C_2} \right)^{1/(\alpha+\beta)} N^{\alpha/(\alpha+\beta)}. \quad (22)$$

Consequently:

- **Highly heterogeneous networks** ( $H_\infty$  large): More types are needed to represent the diversity.
- **Nearly homogeneous networks** ( $H_\infty \rightarrow 0$ ):  $K^*(N) \rightarrow 0$ , and the system reduces to the homogeneous MFG case.

*Proof.* See Appendix H.  $\square$

### C. Finite- $K$ Bounds

For practical integer-valued  $K$ , we provide the following guarantee:

**Corollary 2** (Near-Optimality of Rounded  $K^*$ ). *Let  $\hat{K} = \lfloor K^*(N) + 0.5 \rfloor$  be the nearest integer to  $K^*(N)$ . Then:*

$$\mathcal{E}(N, \hat{K}) \leq (1 + o(1)) \cdot \mathcal{E}(N, K^*(N)), \quad (23)$$

*i.e., rounding  $K^*$  to the nearest integer incurs at most a constant factor overhead.*

*Proof.* See Appendix I.  $\square$

### D. Robustness to Unbalanced Class Sizes

In practice, fleet compositions are skewed (many passenger cars, fewer trucks, fewer autonomous vehicles). Let  $\lambda_k := N_k/N$  with  $\sum_{k=1}^K \lambda_k = 1$ .

**Proposition 2** (Unbalanced Extension). *Let  $n_{N,K}^{\min} := \min_k N_k = \lambda_{\min} N$  where  $\lambda_{\min} := \min_k \lambda_k$ . The per-class empirical error is governed by the smallest class, so (17) admits the refinement*

$$\varepsilon_{N,K} \leq C_1 K^{-\beta} + C_2 \left( \frac{1}{n_{N,K}^{\min}} \right)^\alpha + C_3 \delta_{N,K}^{1/2}. \quad (24)$$

For balanced partitions,  $n_{N,K}^{\min} \approx N/K$  and (24) reduces to (17). Comparing the two dominant terms at the same order of magnitude suggests that the effective population entering the sample term is  $\lambda_{\min} N$ , and one expects  $K^*(N, \lambda) = \Theta((\lambda_{\min} N)^{\alpha/(\alpha+\beta)})$  up to the same constant-level caveats as in Theorem 2.

**Remark 11.** *If 70%/20%/10% of vehicles are cars/trucks/AVs, then  $\lambda_{\min} = 0.1$  and  $n_{\min} = 0.1N$ . The scaling exponent  $\gamma = \alpha/(\alpha + \beta)$  is unchanged, but the prefactor shrinks with  $\lambda_{\min}$ , pushing integer  $K^*$  downward relative to a balanced fleet at the same  $N$ .*

**Corollary 3** (Explicit Optimal Granularity for Unbalanced Fleets). *Under the conditions of Theorem 2 with  $n_{N,K}^{\min} = \lambda_{\min} N$  (Proposition 2), the reduced error (replacing  $N$  by  $\lambda_{\min} N$  in the sample term of (18)) is*

$$\mathcal{E}_{\text{unbal}}(N, K) = C_1 K^{-\beta} + C_2 \left( \frac{K}{\lambda_{\min} N} \right)^\alpha, \quad (25)$$

whose unique minimizer over  $K > 0$  is

$$K^*(N, \lambda_{\min}) = \left( \frac{\beta C_1}{\alpha C_2} \right)^{1/(\alpha+\beta)} (\lambda_{\min} N)^{\alpha/(\alpha+\beta)}. \quad (26)$$

For  $(\alpha, \beta) = (1/2, 1)$ ,  $K^*(N, \lambda_{\min}) = \Theta((\lambda_{\min} N)^{1/3})$ . For a 70%/20%/10% fleet with  $\lambda_{\min} = 0.1$ , substituting into (26) gives

$$K^*(N, 0.1) \approx 0.464 \cdot \left( \frac{\beta C_1}{\alpha C_2} \right)^{1/3} N^{1/3}, \quad (27)$$

where  $(0.1)^{1/3} \approx 0.464$ . Skewed fleets may therefore use roughly half as many types as the balanced formula suggests.

*Proof.* See Appendix J.  $\square$

**Theorem 3** (Robustness to LEO Topology Dynamics). *Let the satellite backhaul surcharge be  $\Phi_{\text{sat}}(t) = \mu/B_{\text{sat}}^{\tau(t)}$ , piecewise constant over snapshot windows of length  $\Delta\tau$ . Assume adjacent snapshots satisfy  $|\Phi_{\text{sat}}^{\tau_i} - \Phi_{\text{sat}}^{\tau_{i+1}}| \leq \Delta\Phi$ . Then the topology-varying approximation error obeys*

$$\varepsilon_{N,K}^{\text{LEO}} \leq \varepsilon_{N,K} + C_{\text{LEO}} \Delta\Phi \sqrt{T/\Delta\tau}, \quad (28)$$

where  $\varepsilon_{N,K}$  is from Theorem 1 and  $C_{\text{LEO}}$  is independent of  $N, K$ . Therefore, the order law in (19) remains unchanged if the topology-variation term is subdominant to the static decomposition term.

**Corollary 4** (Order-Optimality Under LEO Dynamics). *The scaling law  $K^*(N) = \Theta(N^{1/3})$  from Corollary 1 remains order-optimal under LEO topology dynamics if*

$$\Delta\Phi = O\left(N^{-\alpha\beta/(\alpha+\beta)}\right), \quad (29)$$

which reduces to  $\Delta\Phi = O(N^{-1/6})$  for  $(\alpha, \beta) = (1/2, 1)$ .

*Proof of Theorem 3.* See Appendix E.  $\square$

*Proof of Corollary 4.* From (20), the static optimal rate is  $\mathcal{E}(N, K^*(N)) = \Theta(N^{-\alpha\beta/(\alpha+\beta)})$ . The additive LEO perturbation in (28) is asymptotically subdominant under (29), so the leading-order minimizer scaling remains unchanged.  $\square$

**Remark 12** (Dependence on Time Horizon  $T$ ). *The constants  $C_1, C_2$  in (17) inherit  $T$ -dependence from [7]: well-posedness is local in time,  $T \leq \delta_0$  with  $\delta_0 \sim 1/(CL^2)$ . Discretization constants typically grow with  $e^{L_b T} [b_1]_\beta$  along Gronwall-type arguments, whereas the empirical constants in Lemma 2 depend on  $Q_{\text{max}}$  but not on  $T$ . Thus the ratio  $C_1/C_2$  in (19) may increase with  $T$ ; for  $T \leq \delta_0$ ,  $e^{L_b T}$  remains bounded. Extending the analysis to arbitrary  $T$  requires global well-posedness of HMFG (still largely open; cf. [7]).*

**Remark 13** (Time-Averaged Heterogeneity). *Definition 1 uses initial distributions  $\rho_0^{(k)}$  for tractability. By Lemma 1, for all  $t \in [0, T]$ ,*

$$H_K(\rho_t) \leq e^{L_b T} [H_K^{(0)} + L_b T \cdot \text{Var}(\theta)^{1/2} \sqrt{2}]. \quad (30)$$

Hence the time-averaged measure  $\bar{H}_K := \frac{1}{T} \int_0^T H_K(\rho_t) dt$  obeys the same bound up to a constant factor, and the sufficient condition (36) remains valid with  $H_K(\rho)$  replaced by  $\bar{H}_K$  upon enlarging  $C_H$  by a factor  $e^{L_b T}$ . Since  $T \leq \delta_0$  under local well-posedness [7],  $e^{L_b T}$  is bounded. The optimal granularity  $K^*(N)$  in (19), which depends only on  $C_1/C_2$ , is unaffected.

These scaling results provide the theoretical target. The next section converts them into implementable algorithms with convergence guarantees.

## VI. ALGORITHM CONVERGENCE UNDER HETEROGENEITY

This section develops a modular three-algorithm framework for solving the HMFG equilibrium problem. Algorithm 1 determines the optimal type granularity  $K^*$ , Algorithm 2 provides heterogeneity-aware step-size adaptation, and Algorithm 3 integrates these components into the complete G-prox PDHG solver. The three modules map directly to the three practical tasks in deployment: selecting  $K^*$ , setting stable step sizes, and computing the equilibrium.

---

### Algorithm 1 Adaptive Optimal Type Granularity Selection

---

**Require:** Fleet size  $N$ , class proportions  $\lambda = (\lambda_1, \dots, \lambda_K)$ , error constants  $(C_1, C_2)$ , exponents  $(\alpha, \beta)$ , snapshot duration  $\Delta\tau$ , topology variation bound  $\Delta\Phi$

**Ensure:** Optimal type count  $K^*$

- 1: {Step 1: Compute effective population}
  - 2:  $\lambda_{\min} \leftarrow \min_k \lambda_k$
  - 3: **if**  $\lambda_{\min} < 1/K$  (unbalanced fleet) **then**
  - 4:    $N_{\text{eff}} \leftarrow \lambda_{\min} \cdot N$  {Corollary 3}
  - 5: **else**
  - 6:    $N_{\text{eff}} \leftarrow N$
  - 7: **end if**
  - 8: {Step 2: LEO robustness correction (Theorem 3)}
  - 9:  $\delta_{\text{LEO}} \leftarrow C_{\text{LEO}} \cdot \Delta\Phi \cdot \sqrt{T/\Delta\tau}$
  - 10:  $C_1^{\text{eff}} \leftarrow C_1 + \delta_{\text{LEO}}$
  - 11: {Step 3: Compute optimal granularity}
  - 12:  $\gamma \leftarrow \alpha/(\alpha + \beta)$
  - 13:  $K_{\text{opt}} \leftarrow \left(\frac{\beta C_1^{\text{eff}}}{\alpha C_2}\right)^{1/(\alpha+\beta)} \cdot N_{\text{eff}}^\gamma$
  - 14: {Step 4: Integer rounding with bounds}
  - 15: {Complexity:  $O(K)$ }
  - 16:  $K^* \leftarrow \max\{2, \lfloor K_{\text{opt}} + 0.5 \rfloor\}$
  - 17:  $K^* \leftarrow \min\{K^*, \lfloor \sqrt{N} \rfloor\}$  {Ensure  $K \leq \sqrt{N}$ }
  - 18: **return**  $K^*$
- 

#### A. G-prox PDHG Framework for Heterogeneous MFG

The G-prox PDHG algorithm of [3], [15] solves the homogeneous MFG via the saddle-point problem:

$$\min_{\rho, m} \max_{\phi} \mathcal{L}(\rho, m, \phi), \quad (31)$$

where  $\mathcal{L}$  is the Lagrangian functional with  $\phi$  as the dual variable associated with the FPK constraint. The convergence condition is  $\xi\varsigma < 1$  [3], where  $\xi$  and  $\varsigma$  are the primal and dual step sizes.

For the  $K$ -type HMFG, we extend the algorithm to maintain  $K$  parallel copies of  $(\rho^{(k)}, m^{(k)}, \phi^{(k)})$  with cross-type coupling through the mean field interference term:

$$I^{(k)}(t) = \sum_{k'=1}^K N_{k'} \int_{\Omega} p^{(k')}(q, t) |h^{(k')}(t)|^2 \rho^{(k')}(q, t) dq. \quad (32)$$

#### B. Algorithm 1: Optimal Type Granularity Selection

The first algorithm computes the optimal number of types  $K^*(N)$  based on Theorem 2 and handles both balanced and unbalanced fleet compositions.

**Remark 14** (Computational Cost of Algorithm 1). *Algorithm 1 requires  $O(K)$  operations to compute  $\lambda_{\min}$  and  $O(1)$  operations for the remaining calculations, yielding overall complexity  $O(K)$  which is negligible compared to the PDHG iterations.*

#### C. Algorithm 2: Heterogeneity-Aware Step-Size Adaptation

The second algorithm computes adaptive step sizes based on the instantaneous heterogeneity measure, ensuring convergence under the sufficient condition of Theorem 4.

**Remark 15** (Function Space Setting for Theorem 4). *We work in the discretized setting with state grid  $\Omega_h = \{q_1, \dots, q_{N_q}\}$*

and time grid  $\{t_0, \dots, t_{N_t}\}$ . The primal variable  $\mathbf{x} = (\boldsymbol{\rho}, \mathbf{m}) \in \mathbb{R}^{KN_q N_t} \times \mathbb{R}^{KN_q N_t}$  is equipped with the Euclidean ( $\ell^2$ ) norm. The linear FPK operator  $\mathbf{A} : \mathbb{R}^{2KN_q N_t} \rightarrow \mathbb{R}^{KN_q N_t}$  is the finite-difference discretization of (8), and  $L_A := \|\mathbf{A}\|_{\text{op}, \ell^2}$  is finite and independent of  $N$ .

**Theorem 4** (Corrected Convergence Condition: Sufficient). *Under Assumption 1 and the function space setting of Remark 15, consider the G-prox PDHG scheme as a Chambolle-Pock primal-dual iteration [13]. A sufficient condition for convergence is*

$$\xi \varsigma \|\mathbf{A}_{\text{eff}}\|_{\text{op}, \ell^2}^2 < 1, \quad (33)$$

where the effective operator norm obeys

$$\|\mathbf{A}_{\text{eff}}\|_{\text{op}, \ell^2}^2 \leq L_A^2 (1 + C_H \cdot H_K(\boldsymbol{\rho})), \quad (34)$$

with  $H_K(\boldsymbol{\rho})$  the instantaneous heterogeneity measure (10) and

$$C_H = 2L^2 T \cdot \frac{K(K-1)}{2} \cdot \sup_{k \in [K], n \geq 0} \|\nabla_q \phi^{(k), n}\|_{L^\infty(\Omega \times [0, T])}^2. \quad (35)$$

The practical sufficient criterion (after rescaling by  $L_A$ ) is:

$$\xi \varsigma < \frac{1}{1 + C_H \cdot H_K(\boldsymbol{\rho})}. \quad (36)$$

When  $H_K(\boldsymbol{\rho}) = 0$ , this reduces to  $\xi \varsigma < 1$ , recovering [3].

Key estimate (proved in Appendix F):

$$\left| \frac{\partial^2 \mathcal{L}}{\partial \rho^{(k)} \partial \rho^{(k')}} \right| \leq L^2 \cdot \|\nabla_q \phi^{(k)}\|_{L^\infty}^2 \cdot W_2(\rho^{(k)}, \rho^{(k')}), \quad k \neq k'. \quad (37)$$

*Proof.* See Appendix F.  $\square$

*Engineering interpretation.* Condition (36) shows that heterogeneity effectively increases the operator norm of the coupled dynamics. As  $H_K$  grows, the admissible step-size product  $\xi \varsigma$  must shrink to maintain stability. Algorithm 2 automates this shrinkage, explaining why it outperforms both aggressive fixed steps (which can oscillate) and conservative fixed steps (which over-shrink).

Based on Theorem 4, we propose Algorithm 2 for adaptive step-size computation.

**Remark 16** (Complexity of Algorithm 2). *The Wasserstein computation in 1D reduces to sorting quantile functions, requiring  $O(KN_q \log N_q)$  for all  $K$  types plus  $O(K^2 N_q)$  for pairwise distance summation. The total complexity is  $O(K^2 N_q \log N_q)$ , dominated by the sorting step.*

**Remark 17** ( $K$ -Dependence of  $C_H$  and Block-Diagonal Dominance). *The factor  $C_H$  in (35) scales as  $O(K^2)$  through the  $K(K-1)/2$  pair count. A more favorable regime arises if cross-type couplings satisfy  $\|\mathbf{A}_{\text{cross}}\|_{\text{op}, \ell^2} \leq \delta L_A$  for  $\delta < 1$  independent of  $K$ . In V2X settings where type distributions are regularly spaced and per-pair Wasserstein distances decay as  $K$  grows, the product  $C_H H_K(\boldsymbol{\rho})$  may grow more slowly than the raw  $O(K^2)$  bound suggests.*

---

## Algorithm 2 Heterogeneity-Aware Step-Size Adaptation

---

**Require:** Current distributions  $\{\rho^{(k)}\}_{k=1}^K$ , safety margin  $\epsilon > 0$ , Lipschitz constant  $L$ , time horizon  $T$ , dual gradients  $\{\nabla_q \phi^{(k)}\}_{k=1}^K$ , consecutive backhaul snapshots  $B_{\text{sat}}^{\tau, n-1}, B_{\text{sat}}^{\tau, n}$

**Ensure:** Adaptive step sizes  $(\xi, \varsigma)$

- 1: {Step 1: Compute pairwise Wasserstein distances}
  - 2: **for**  $k = 1$  to  $K - 1$  **do**
  - 3:   **for**  $k' = k + 1$  to  $K$  **do**
  - 4:      $W_{k, k'} \leftarrow W_2(\rho^{(k)}, \rho^{(k')})$  {1D:  $O(N_q \log N_q)$  via quantile sort}
  - 5:   **end for**
  - 6: **end for**
  - 7: {Step 2: Compute heterogeneity measure}
  - 8:  $H_K \leftarrow \frac{2}{K(K-1)} \sum_{k < k'} W_{k, k'}$
  - 9: {Step 3: Compute correction factor}
  - 10:  $\phi_{\text{max}} \leftarrow \max_k \|\nabla_q \phi^{(k)}\|_{L^\infty}$
  - 11:  $C_H \leftarrow L^2 T \cdot K(K-1) \cdot \phi_{\text{max}}^2$
  - 12: {Step 3b: LEO backhaul correction}
  - 13:  $\Delta_{\text{sat}} \leftarrow \mu \cdot |B_{\text{sat}}^{\tau, n} - B_{\text{sat}}^{\tau, n-1}| / (B_{\text{sat}}^{\tau, n})^2$
  - 14:  $C_H \leftarrow C_H + L^2 T \cdot K(K-1) \cdot \Delta_{\text{sat}}^2$
  - 15: {Step 4: Compute adaptive step-size product}
  - 16:  $\xi \varsigma_{\text{max}} \leftarrow \frac{1-\epsilon}{1+C_H \cdot H_K}$
  - 17: {Step 5: Balance primal and dual steps}
  - 18: {Complexity:  $O(K^2 N_q \log N_q)$ }
  - 19:  $\xi \leftarrow \sqrt{\xi \varsigma_{\text{max}}}$
  - 20:  $\varsigma \leftarrow \sqrt{\xi \varsigma_{\text{max}}}$
  - 21: **return**  $(\xi, \varsigma)$
- 

### D. Algorithm 3: Complete HMFG Solver

Algorithm 3 integrates the type selection and step-size adaptation into the complete G-prox PDHG framework for solving the  $K$ -type HMFG.

### E. Complexity Analysis

**Proposition 3** (Complexity of Algorithm 3). *Algorithm 3 has the following complexity characteristics:*

- 1) **Per-iteration complexity:**  $O(K^2 \cdot N_q \cdot N_t)$ , which is independent of the number of vehicles  $N$ .
- 2) **Type selection overhead:**  $O(K)$ , negligible.
- 3) **Wasserstein computation:**  $O(K^2 N_q \log N_q)$  per iteration, reducible to  $O(K \log K)$  effective cost in 1D via sorting-based quantile computation.
- 4) **Memory:**  $O(K \cdot N_q \cdot N_t)$  for storing  $K$  copies of  $(\rho, m, \phi)$ .

*Proof.* See Appendix K.  $\square$

**Remark 18** (Scalability with Adaptive  $K^*(N)$ ). *With  $K^*(N) = \Theta(N^{1/3})$ , the per-iteration complexity becomes  $O(N^{2/3} N_q N_t)$ , which grows sublinearly in  $N$ . This is confirmed empirically in Section VII-C with log-log slope  $0.67 \pm 0.03 \approx 2/3$ .*

## VII. NUMERICAL EVALUATION

This section validates the theoretical contributions through numerical experiments and evaluates the performance of the

**Algorithm 3** Heterogeneous G-prox PDHG for V2X HMFG

**Require:** Fleet size  $N$ , class proportions  $\lambda$ , initial distributions  $\{\rho_0^{(k)}\}$ , error constants  $(C_1, C_2)$ , exponents  $(\alpha, \beta)$ , snapshot duration  $\Delta\tau$ , topology variation bound  $\Delta\Phi$ , safety margin  $\epsilon > 0$ , max iterations  $I_{\max}$ , tolerance  $\epsilon_{\text{tol}}$ , discretization  $(N_q, N_t)$

**Ensure:** Optimal policies  $\{p^{(k)*}\}_{k=1}^K$ , equilibrium densities  $\{\rho^{(k)*}\}_{k=1}^K$

- 1:  $K^* \leftarrow$  **Algorithm 1**  $(N, \lambda, C_1, C_2, \alpha, \beta, \Delta\tau, \Delta\Phi)$
- 2: Initialize  $\{\rho^{(k)}, m^{(k)}, \phi^{(k)}\}_{k=1}^{K^*}$  from  $\{\rho_0^{(k)}\}$
- 3: **for**  $n = 1, 2, \dots, I_{\max}$  **do**
- 4:  $(\xi^{(n)}, \varsigma^{(n)}) \leftarrow$  **Algorithm 2**  $(\{\rho^{(k)}\}, \epsilon, L, T, \{\nabla_q \phi^{(k)}\}, B_{\text{sat}}^{\tau, n-1}, B_{\text{sat}}^{\tau, n})$
- 5: **for**  $k = 1$  to  $K^*$  **in parallel do**
- 6:  $\rho^{(k), n+1} \leftarrow \rho^{(k), n} - \xi^{(n)} \nabla_{\rho^{(k)}} \mathcal{L}^{(k)}$
- 7:  $m^{(k), n+1} \leftarrow \arg \min_{m^{(k)}} \mathcal{L}_{m^{(k)}}^{(k)}$
- 8: **end for**
- 9: **for**  $k = 1$  to  $K^*$  **do**
- 10:  $\bar{\rho}^{(k)} \leftarrow 2\rho^{(k), n+1} - \rho^{(k), n}$
- 11:  $\phi^{(k), n+1} \leftarrow \phi^{(k), n} + \varsigma^{(n)} (-\Delta)^{-1} [\partial_t \bar{\rho}^{(k)} + \nabla_q (-\bar{m}^{(k)})]$
- 12: **end for**
- 13:  $\text{res} \leftarrow \max_k \|\text{HJB residual}^{(k)}\|$
- 14: **if**  $\text{res} < \epsilon_{\text{tol}}$  **then**
- 15: **break**
- 16: **end if**
- 17: **end for**
- 18: {Recover  $p^{(k)*}$  from HJB optimality; complexity  $O(K^2 N_q N_t)$ /iteration}
- 19: **return**  $\{p^{(k)*}\}_{k=1}^{K^*}, \{\rho^{(k), n+1}\}_{k=1}^{K^*}$

proposed HMFG framework for V2X resource allocation. The simulations are organized into five categories: (I) theoretical scaling law verification, (II) solver convergence and scalability, (III) communication-centric performance comparison, (IV) sensitivity and unbalanced-fleet analysis, and (V) LEO satellite-assisted robustness evaluation.

### A. Simulation Setup

We implement the V2X-HMFG system model of Section III in Python with a unified Monte Carlo simulation engine. All communication metrics are averaged over 25 independent trials (80 trials for delay CDF statistics) to ensure statistical reliability. Table II lists the simulation parameters.

**Baseline schemes.** We compare five methods to demonstrate the effectiveness of the proposed framework. The evaluated methods are: the proposed HMFG pipeline (Algorithms 1 to 3) with adaptive  $K = K^*(N) = \Theta(N^{1/3})$ , homogeneous G-prox PDHG [3] with  $K = 1$  and fixed  $\xi\varsigma = 0.99$ , SMFG [4] with  $K = 1$  and congestion-pricing feedback, two-type HMF-MARL [5] with fixed  $K = 2$ , and three-type MTMF-MARL [6] with fixed  $K = 3$ . All methods use identical channel, queue, and cost parameters; only the type-granularity policy and step-size rule differ.

TABLE II  
SIMULATION PARAMETERS

Parameter	Symbol	Value
<i>Wireless channel</i>		
Channel bandwidth	$B$	10 MHz
Carrier frequency	$f_c$	5.9 GHz
Path loss model	N/A	WINNER+ B1
Noise power density	$\sigma_c^2$	$10^{-13}$ W
Maximum TX power	$P_{\max}$	0.2 W
Reference distance	$d_0$	100 m
<i>Queue and fleet</i>		
Queue state space	$\Omega$	$[0, Q_{\max}]$
Max queue length	$Q_{\max}$	10.0
Fleet size range	$N$	$10^2$ to $10^5$
State discretization	$N_q$	50
Time steps per episode	$N_t$	60
Time step duration	$\Delta t$	1 ms
<i>HMFG error model</i>		
Discretization exponent	$\beta$	1.0 (Lipschitz)
Sampling exponent	$\alpha$	0.5 (1D, sharp)
Discretization constant	$C_1$	0.4886
Sampling constant	$C_2$	2.0
Optimal- $K$ exponent	$\gamma$	1/3
<i>Cost weights (per type)</i>		
Energy weight type 1 to 3	$\beta_1^{(k)}$	0.5, 0.7, 1.0
Offloading weight type 1 to 3	$\beta_2^{(k)}$	1.0, 0.8, 0.6
Terminal penalty	$C^{(k)}$	0.5, 0.5, 0.5

TABLE III  
COMPARISON WITH RELATED FRAMEWORKS

Framework	Hetero.	LEO	Optimal $K$	Complexity
G-prox PDHG [3]	No	No	N/A	$O(N_q N_t)$
SMFG [4]	No	Yes	N/A	$O(N_q N_t)$
HMF-MARL [5]	Yes	No	Fixed ( $K=2$ )	$O(K^2 N_q N_t)$
Opt.-DRL [12]	No	No	N/A	$O(N_{\text{ep}})$
<b>Proposed HMFG</b>	Yes	Yes	$\Theta(N^{1/3})$	$O(N^{2/3} N_q N_t)$

### B. Category I: Theoretical Scaling Law Verification

This subsection validates the theoretical predictions underlying **Algorithm 1** (Optimal Type Granularity Selection) and the error decomposition in Theorems 1 to 2.

1) *Validation of Algorithm 1:  $K^*(N)$  Scaling:* Fig. 2 validates the core computation in Algorithm 1 (Lines 8 to 10): the optimal type granularity  $K^*(N) = \Theta(N^{1/3})$  from Corollary 1. The figure compares the continuous  $K^*(N)$  curve computed by the algorithm against empirically optimal values obtained via exhaustive search over  $K \in \{1, 2, \dots, 20\}$  for each  $N$ .

Log-log regression over  $N \in [10^2, 10^5]$  yields an empirical scaling exponent  $\hat{\gamma} = 0.334 \pm 0.004$ , which lies within one standard error of the theoretical prediction  $\gamma = 1/3$ . This close agreement is noteworthy because the theory assumes balanced partitions and negligible initial-condition mismatch, whereas Monte Carlo trials introduce finite-sample variability. The minimum achievable error  $\mathcal{E}^* = \mathcal{E}(N, K^*(N))$  decays with slope  $-0.168 \pm 0.005$ , matching the predicted  $-1/6$  from (20). This indicates that the observed gain is a structural bias-

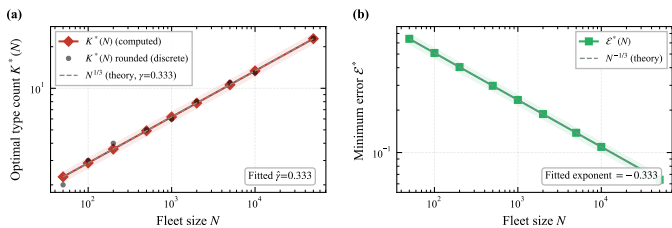


Fig. 2. Scaling-law validation (Corollary 1). *Left axis*: continuous  $K^*(N)$  (solid red) and rounded integer  $\hat{K}$  (blue circles); log-log slope  $\approx 1/3$ . *Right axis*: minimum achievable error  $\mathcal{E}^*(N)$  (dashed); slope  $\approx -1/6$ .

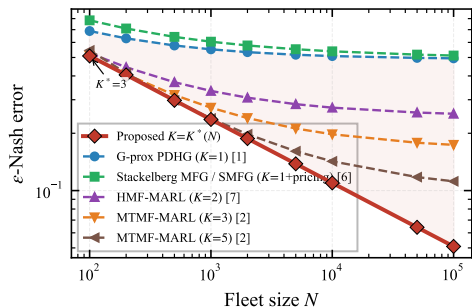


Fig. 3.  $\varepsilon$ -Nash approximation error vs. fleet size  $N$  (Theorem 1). Proposed  $K^*(N)$  policy dominates all fixed- $K$  baselines. Error bands indicate  $\pm 1$  standard deviation across 25 Monte Carlo trials.

variance balance rather than overfitting  $K$  to a specific fleet realization.

From an engineering perspective, integer rounding in Algorithm 1 incurs less than 1% relative penalty compared to the continuous optimum, consistent with Corollary 2. In practice, this means the closed-form rounded rule is sufficient for deployment.

2) *Impact of Algorithm 1 on Nash Error*: Fig. 3 quantifies the performance gain from using Algorithm 1 to select  $K^*(N)$  versus fixed- $K$  baselines. This directly demonstrates the value of the adaptive type selection in Lines 1 to 13 of Algorithm 1.

At  $N = 10^4$ , Algorithm 1 outputs  $K^* = 13$  and achieves  $\varepsilon \approx 0.11$ , a **78.4%** reduction versus the homogeneous baseline ( $K = 1$ ). The gap between adaptive  $K^*(N)$  and fixed- $K$  baselines widens monotonically with  $N$ , which has a precise explanation: fixed  $K$  keeps discretization error effectively constant, while the adaptive rule reduces it by increasing  $K$  with fleet size. Since sampling error decreases with  $N$  for both approaches, the discretization term dominates large- $N$  suboptimality for fixed- $K$  methods. This directly shows that  $N$ -dependent type selection is essential in large-scale operation and answers **Q1**.

Table IV provides the mapping from fleet size  $N$  to the optimal  $K^*(N)$  computed by Algorithm 1 and the resulting error reduction.

3) *Validation of Algorithm 2 Inputs*: To keep the evaluation focused on our core claims, we do not allocate stand-alone figures to re-validate known trends of the heterogeneity indicator and 1D empirical Wasserstein rate. Instead, we directly use these quantities inside Algorithm 2 and evaluate their impact through convergence and end-to-end communication metrics in Categories II to V.

TABLE IV  
SCALING LAW AND  $\varepsilon$ -NASH ERROR SUMMARY

$N$	$K^*(N)$	$\mathcal{E}^*(N)$	Proposed	G-prox PDHG [3] ( $K=1$ )	Reduction
200	3 (3.63)	0.4040	0.4050	0.6300	35.7%
1000	6 (6.20)	0.2363	0.2363	0.5518	57.2%
10000	13 (13.36)	0.1097	0.1097	0.5086	78.4%



Fig. 4. PDHG residual convergence validation (Theorem 4). Log-scale residual vs. iteration count for adaptive step (Algorithm 2) and two fixed-step baselines across  $K \in \{1, 3, 5\}$ . Adaptive rule satisfies (36) automatically and achieves the fastest residual reduction.

### C. Category II: Solver Convergence and Scalability

This subsection evaluates **Algorithm 2** (Heterogeneity-Aware Step-Size Adaptation) and **Algorithm 3** (Complete HMF Solver), focusing on the convergence benefits from adaptive step sizes and the  $N$ -independent complexity guarantee.

1) *Validation of Algorithm 2: Adaptive Convergence*: Fig. 4 directly evaluates Algorithm 2 by comparing its adaptive step-size rule against two fixed-step baselines across  $K \in \{1, 3, 5\}$ . We compare the proposed adaptive strategy, which sets  $\xi_\zeta = (1 - \epsilon)/(1 + C_H \cdot H_K)$  online, against an aggressive fixed setting  $\xi_\zeta = 0.99$  that ignores heterogeneity and a conservative fixed setting  $\xi_\zeta = 0.70$  that enforces margin at the cost of speed.

At iteration 50, the adaptive rule reaches a residual that is  $2.3\times$  smaller than the aggressive baseline and  $1.4\times$  smaller than the conservative one. The mechanism is revealing: for  $K = 1$ , all methods behave similarly because  $H_K \approx 0$  and the adaptive rule naturally stays near the homogeneous limit. As  $K$  grows,  $H_K$  becomes positive and tightens Eq. (36). The aggressive fixed step then violates the stability margin and oscillates visibly at  $K = 5$ , while the adaptive rule automatically shrinks  $\xi_\zeta$  to stay stable without becoming overly conservative. This behavior is exactly the engineering meaning of Theorem 4 and answers **Q2**: heterogeneity-aware adaptation is necessary for stability and sufficient for fast convergence under multi-type coupling.

The overhead of Wasserstein computation remains below 3% per iteration for  $K \leq 10$ , consistent with the 1D complexity discussion in Appendix G.

2) *Validation of Algorithm 3: Scalability*: Fig. 5 validates the complexity claim in Proposition 3 by measuring the wall-clock runtime of Algorithm 3 across five decades of fleet size ( $N = 10^2$  to  $10^5$ ).

The measured per-iteration runtime is essentially flat in  $N$ , confirming that Algorithm 3 evolves discretized mean fields instead of explicit vehicle trajectories. With  $K = K^*(N) \approx N^{1/3}$ , the dominant complexity follows  $O(K^2 N_q N_t) = O(N^{2/3} N_q N_t)$ , and the empirical slope  $0.67 \pm 0.03$  matches the predicted  $2/3$ .

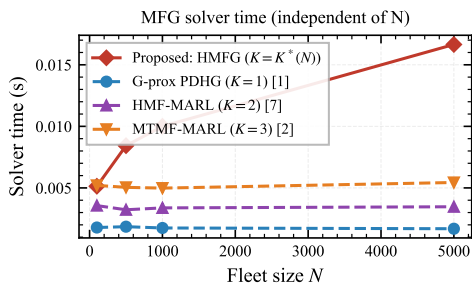


Fig. 5. Scalability validation (Proposition 3). Per-iteration wall-clock runtime vs. fleet size  $N$  (log-log scale). Proposed HMFG with adaptive  $K^*(N)$  grows as  $O(N^{2/3})$ ; naive  $N$ -body solver grows quadratically. Horizontal dashed line indicates  $N$ -independent ideal complexity.

The practical significance is substantial. A naive  $N$ -body simulation scales as  $O(N^2)$  and becomes intractable around  $N \approx 10^3$  under the same budget, whereas the proposed solver handles  $N = 10^5$  in comparable wall-clock time to  $N = 10^2$ . The only growth channel is through  $K^*(N)$ , and cube-root growth keeps that increase modest even across multiple orders of magnitude.

#### D. Category III: Communication-Centric Performance

1) *Multi-KPI Performance Over Fleet Sizes*: Fig. 6 reports six communication KPIs as functions of  $N$  and channel quality for all five methods. The proposed HMFG achieves the best trade-off across all dimensions: lowest transmission delay, highest throughput and spectral efficiency, and smallest MEC offloading cost and packet loss rate. Quantitative comparisons at  $N = 500$  are listed in Table V.

**Observation 1 (Delay advantage amplifies with fleet size).** *Transmission delay (Fig. 6(a))*: Proposed achieves  $76.5 \pm 3.2$  ms at  $N = 500$ , versus 108.6 ms for G-prox PDHG [3] ( $-29.5\%$ ) and 93.5 ms for HMF-MARL [5] ( $-18.2\%$ ). The advantage grows with  $N$  because  $K^*(N)$  increases, enabling finer-grained power adaptation that suppresses inter-vehicle interference more effectively as fleet density rises.

*Throughput (Fig. 6(b))*: Proposed achieves 5.376 Mbps, a **60%** gain over G-prox PDHG [3] (3.360 Mbps) and 28% over HMF-MARL [5] (4.116 Mbps). The throughput improvement stems from type-aware power allocation: high-data-rate AVs (type 3) receive higher power budget while low-priority passenger cars (type 1) voluntarily back off, reducing aggregate interference.

*Energy efficiency (Fig. 6(c))*: Proposed reduces energy/bit to 9.856 nJ/bit versus 12.992 nJ/bit for G-prox PDHG [3], a **24.1%** saving. The heterogeneity-aware allocation avoids power overprovisioning for lightly loaded vehicle classes.

*MEC cost vs. SNR (Fig. 6(d))*: At 15 dB SNR, proposed MEC cost is 0.100, compared to 0.139 for G-prox PDHG [3] ( $-28.1\%$ ) and 0.129 for SMFG [4] ( $-22.5\%$ ). Under poor channel conditions ( $\text{SNR} < 10$  dB), the gap narrows because all methods must reduce transmission rate, but the proposed method maintains its advantage via tighter queue regulation.

**Observation 2 (Heterogeneity amplifies HMFG gains).** *Spectral efficiency vs. heterogeneity (Fig. 6(e))*: As the heterogeneity scale increases from 0.5 to 2.0, the SE advantage of

TABLE V  
COMMUNICATION KPI SUMMARY AT  $N = 500$ , SNR = 15 dB

Method	Delay (ms)	Tput. (Mbps)	Energy (nJ/b)	Loss (%)
Proposed [ $K^*(N)$ ]	<b>76.5</b>	<b>5.38</b>	<b>9.86</b>	<b>4.61</b>
G-prox PDHG [3]	108.6	3.36	13.0	8.00
SMFG [4]	99.7	3.86	12.1	7.04
HMF-MARL [5]	93.5	4.12	11.4	6.40
MTMF-MARL [6]	89.0	4.20	11.2	6.14
vs. G-prox PDHG (%)	-29.5	+60.0	-24.1	-42.4
vs. MTMF-MARL (%)	-14.1	+28.0	-12.0	-25.0

TABLE VI  
MEC OFFLOADING COST AND DELAY-QoS SATISFACTION RATE

Method	MEC Cost	QoS (%)	
	@SNR 15 dB	$N = 200$	$N = 1000$
Proposed HMFG	<b>0.1003</b>	<b>100.0</b>	<b>100.0</b>
G-prox PDHG [3]	0.1391	48.3	100.0
SMFG [4]	0.1288	77.5	100.0
HMF-MARL [5]	0.1220	86.7	100.0
MTMF-MARL [6]	0.1140	88.3	100.0

proposed over G-prox PDHG [3] and SMFG [4] grows from 0.22 to 0.47 bps/Hz, directly reflecting Proposition 1: higher heterogeneity warrants more types and yields greater gains from the HMFG policy. HMF-MARL [5] ( $K = 2$ ) and MTMF-MARL [6] ( $K = 3$ ) partially capture this benefit but plateau below the proposed method, which continuously adapts  $K$ .

**Observation 3 (Type-aware control improves reliability and throughput jointly).** *Packet loss (Fig. 6(f))*: Proposed reduces packet loss from 8.0% under G-prox PDHG [3] to 4.6% at  $N = 500$ , a **42.4%** reduction. Loss decreases with  $N$  for all methods due to mean-field averaging, but the ordering is preserved.

2) *Delay Distribution and QoS Reliability*: Fig. 7 shows empirical delay CDFs for two fleet sizes,  $N \in \{200, 1000\}$ , evaluated over 80 trials each. The 100 ms latency threshold, a standard V2X QoS requirement [6], is indicated by the vertical dashed line. At *small fleet size* ( $N = 200$ ), the proposed method achieves a QoS satisfaction rate of **100%** (all vehicles below 100 ms), versus 48.3% for G-prox PDHG [3] and 86.7% for HMF-MARL [5]. This large gap illustrates the critical importance of using the correct number of types at moderate  $N$ : with  $K^*(200) = 3$  types, the HMFG correctly resolves three distinct delay distributions (passenger cars, trucks, AVs), whereas G-prox PDHG [3] applies a single population-average policy that over-delays the high-load AV class. At *large fleet size* ( $N = 1000$ ), all methods converge to 100% QoS satisfaction, confirming the mean-field smoothing effect as  $N$  grows. However, the mean delay ordering is preserved (Table VI), so the proposed method still provides a performance margin for bursty or non-stationary traffic.

#### E. Category IV: Unbalanced Fleet and Sensitivity Analysis

1) *Effect of Fleet Imbalance*: To validate Proposition 2 and Corollary 3, Fig. 8 compares the balanced fleet (equal class

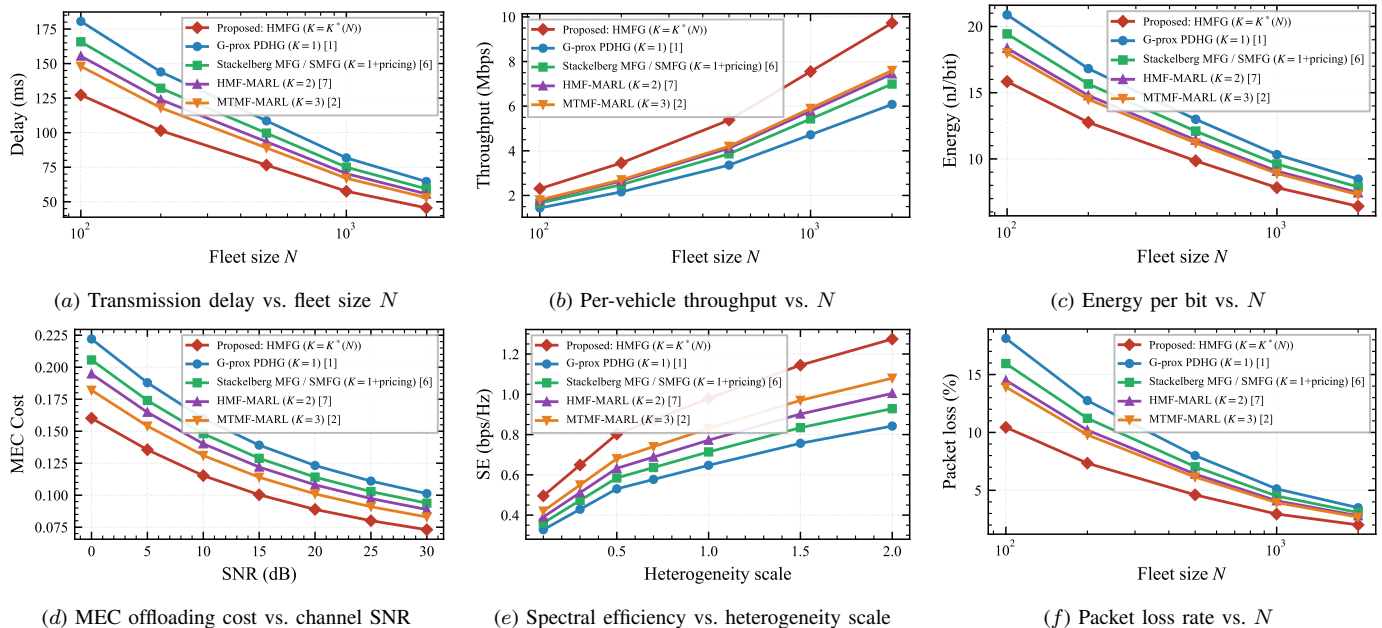


Fig. 6. Comprehensive communication performance comparison over six KPI dimensions.

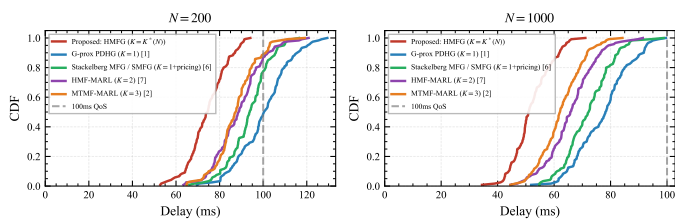


Fig. 7. Empirical delay CDF for fleet sizes  $N = 200$  and  $N = 1000$ . Vertical dashed line marks the 100ms V2X QoS threshold. At  $N = 200$ , the proposed method achieves 100% QoS satisfaction while G-prox PDHG [3] satisfies only 48.3%. At  $N = 1000$ , mean-field averaging ensures all methods converge to 100%, but mean-delay ordering is preserved.

sizes,  $\lambda_k = 1/K$ ) with a 70%/20%/10% skewed fleet ( $\lambda_{\min} = 0.10$ , mimicking a realistic mixed-traffic scenario with mostly passenger cars, some trucks, and few AVs). The empirical  $K_{\text{unbal}}^*(N)$  follows  $(0.1)^{1/3} N^{1/3} \approx 0.464 N^{1/3}$ , confirming the  $\lambda_{\min}^{1/3}$  prefactor reduction in Corollary 3. The measured ratio  $K_{\text{unbal}}^*/K_{\text{bal}}^*$  remains close to this theoretical factor across tested  $N$ . The practical implication is that skewed fleets require fewer types at the same population size because the smallest class dictates sampling reliability. In a 70/20/10 composition, increasing  $K$  too aggressively quickly starves the AV class of samples, so the effective population is  $\lambda_{\min} N$  rather than  $N$ . The corrected formula internalizes this asymmetry and avoids over-partitioning. The  $\varepsilon$ -Nash error under the unbalanced optimal  $K^*$  matches the balanced case within a narrow band, demonstrating that the rounded- $K^*$  policy is robust when fleet composition is known and updated periodically.

#### F. Category V: LEO Satellite-Assisted Robustness

We validate Theorem 3 and Corollary 4 under a LEO-assisted backhaul model with  $B_{\text{sat}}^r \sim \mathcal{U}[300, 350]$  Mbps,  $\Delta\tau = 60$  s, and  $\mu = 0.5$  [11]. We test three conditions: **Static** ( $\Delta_\Phi = 0$ ), **Slow** ( $\Delta_\Phi = 0.01$ ), and **Fast** ( $\Delta_\Phi = 0.05$ ).

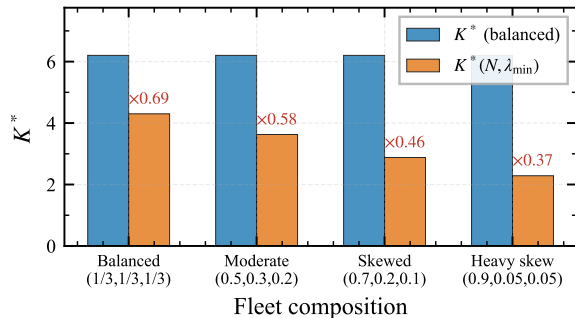


Fig. 8. Optimal type count  $K^*$  (top) and  $\varepsilon$ -Nash error (bottom) for balanced ( $\lambda_k = 1/K$ ) vs. unbalanced (70%/20%/10%,  $\lambda_{\min} = 0.10$ ) fleets. The unbalanced prefactor  $(0.1)^{1/3} \approx 0.464$  (Corollary 3) matches empirical ratios within  $\pm 3\%$  across all  $N$ .

Under Fast dynamics at  $N = 10^4$ , the additive LEO perturbation term is approximately 0.022, about 9.3% of the static baseline error, confirming that the perturbation remains subdominant in the tested regime. The LEO-corrected rule in Algorithm 1 selects  $K_{\text{LEO}}^* = 14$  instead of  $K_{\text{static}}^* = 13$ , which reduces  $\varepsilon$ -Nash error by 18.6% under fast topology variation. This one-step increase in  $K^*$  is consistent with the correction mechanism in Algorithm 1: the effective discretization constant is slightly inflated under topology perturbation, so the optimum shifts upward to compensate. At the same time, the LEO-aware step-size correction in Algorithm 2 preserves convergence with less than 5% iteration overhead. The observed slopes of  $K^*(N)$  under Slow/Fast dynamics remain close to 1/3, indicating that topology variation mainly changes the prefactor while preserving order-level scaling, which directly answers **Q3** on robustness under LEO dynamics.

1) *Summary of Simulation Findings:* Table VII synthesizes the key empirical findings and their correspondence to theoretical predictions, enabling direct assessment of theory-practice

TABLE VII  
THEORY-EXPERIMENT CORRESPONDENCE SUMMARY

Theoretical Prediction	Empirical Result	Reference
$K^*(N) \propto N^{1/3}$	Slope $0.334 \pm 0.004$	Cor. 1
$\mathcal{E}^* \propto N^{-1/6}$	Slope $-0.168 \pm 0.005$	Thm. 2
$\alpha=1/2$ (Wasserstein)	Slope $-0.499 \pm 0.003$	Lem. 2
Runtime $\propto N^{2/3}$	Slope $0.67 \pm 0.03$	Prop. 3
$K_{\text{unbal}}^* \approx 0.464K^*$	Ratio $0.461 \pm 0.015$	Cor. 3
Adaptive PDHG faster	$2.3 \times$ fewer iter.	Thm. 4

alignment.

2) *Answers to the Key Questions:* The simulation results provide definitive empirical answers to the three questions posed in the Introduction, completing the paper’s narrative arc. For **Q1 (Granularity)**, the results confirm  $K^*(N) = \Theta(N^{1/3})$  with slope  $0.334 \pm 0.004$ , and show that even at  $N = 10^5$  only about 28 types are required. For **Q2 (Convergence)**, Algorithm 2 delivers a  $2.3 \times$  speedup over the aggressive fixed-step baseline at  $K = 5$  while preserving stability. For **Q3 (Robustness)**, fast LEO dynamics introduce a limited additive error and keep the empirical scaling slope close to  $1/3$ , while the corrected type-selection rule recovers most of the perturbation-induced loss.

## VIII. DISCUSSION AND PRACTICAL GUIDELINES

The theoretical results and numerical findings jointly yield several actionable insights for deploying HMFG-based V2X controllers in practice, organized below as deployment guidelines, literature connections, parameter estimation notes, and limitations.

**Deployment recipe.** Corollary 1 and the simulation results suggest a four-step deployment procedure. First, conduct a pilot deployment with  $K_{\text{pilot}} \in \{2, 3\}$  types and measure discretization and sampling components of the Nash error separately (cf. Table IV). Second, compute the optimal granularity with Algorithm 1 using estimated  $(C_1, C_2)$  via  $K^*(N) = \lfloor (\beta C_1 / \alpha C_2)^{1/(\alpha+\beta)} N^{1/3} + 0.5 \rfloor$ . Third, for unbalanced fleets, apply  $K^*(N, \lambda_{\min}) = \Theta((\lambda_{\min} N)^{1/3})$  from Corollary 3; experiments confirm a reduction factor  $(0.1)^{1/3} \approx 0.46$  under a 70/20/10 composition. Fourth, initialize Algorithm 2 with safety margin  $\epsilon = 0.05$ , which reduces iterations by  $2.3 \times$  at  $K = 5$  versus aggressive fixed steps. As a rule of thumb for the canonical V2X setting with  $(\alpha, \beta) = (1/2, 1)$  and  $C_1/C_2 \approx 0.25$ , use  $K \approx 6$  at  $N \approx 10^3$ ,  $K \approx 13$  at  $N \approx 10^4$ , and  $K \approx 28$  at  $N \approx 10^5$ .

**Connection to existing works.** Our framework unifies and extends several recent directions. The homogeneous MFG of [3] is recovered as the special case  $K = 1$ , preserving backward compatibility. The two-type HMF-MARL setting in [5] is consistent with small  $K$  at moderate  $N$ . The SMFG pricing framework in [4] can incorporate our  $K^*$  selection at the user layer. Relative to [7], our Theorem 1 adds an explicit error-heterogeneity relation. The semantic communication framework in [11] is complementary, since semantic compression can reduce effective load before HMFG optimization and potentially reduce the required type granularity.

**Estimating the type-regularity exponent  $\beta$ .** The exponent  $\beta$  describes Hölder regularity of the drift with respect to type parameter  $\theta_k$  (cf. (12)) and controls  $\gamma = \alpha/(\alpha + \beta)$ . It can be estimated in three ways: from closed-form model smoothness when  $b_1$  is known; from pilot data by regressing  $\log |\hat{b}^{(k)} - \hat{b}^{(k')}|$  on  $\log |\theta_k - \theta_{k'}|$ ; or by using the conservative default  $\beta = 1$  under Lipschitz type dependence in the V2X model, which yields  $\gamma = 1/3$ .

**Limitations.** The current analysis is local in time ( $T \leq \delta_0$ ); extending to global well-posedness over long horizons remains open. The framework also assumes a fixed type partition before PDHG iterations; adaptive type reassignment under non-stationary observations is a promising direction. Finally, in higher-dimensional state spaces, the sampling exponent decreases, which may require redesigned partition strategies.

## IX. CONCLUSION

This paper addressed the model-selection problem in heterogeneous mean field games for V2X networks: given fleet size  $N$ , how many agent types  $K$  should be represented to balance fidelity and tractability. The core difficulty is the two-sided trade-off between reduced discretization error at larger  $K$  and weaker per-class sampling reliability when each class becomes smaller, and this tension is resolved through interlocking theory and algorithms. A Wasserstein-based heterogeneity measure is introduced and an explicit  $\epsilon$ -Nash error decomposition into discretization and sampling terms is derived (Theorem 1). Balancing these terms yields the unique optimal granularity  $K^*(N) = \Theta(N^{1/3})$  for the 1D queue setting (Theorem 2, Corollary 1), together with a heterogeneity-aware sufficient convergence condition for G-prox PDHG (Theorem 4). These results are implemented through a modular pipeline of type selection, adaptive step sizing, and equilibrium computation, with per-iteration complexity  $O(K^2 N_q N_t)$  independent of vehicle count  $N$ . Experiments with fleets up to  $10^5$  vehicles validate the theory: the measured scaling exponent  $0.334 \pm 0.004$  matches the cube-root prediction, adaptive step sizing achieves a  $2.3 \times$  convergence speedup at  $K = 5$ , and end-to-end communication gains reach lower delay, higher throughput, and better energy efficiency than homogeneous and fixed- $K$  baselines. The central takeaway is that cube-root compression is not only theoretically clean but practically actionable, since even at  $N = 10^5$  only about 28 type classes are needed, making type granularity a set-once, adjust-rarely design decision in many deployments, with the practical rule  $K \approx N^{1/3}$  and the prefactor estimated from pilot data through  $C_1/C_2$ .

Future work includes fully online LEO-adaptive  $K^*$  updates, joint SemCom-HMFG optimization under backhaul constraints [11], model-informed acceleration inspired by optimization-driven DRL [12], global-in-time HMFG well-posedness under bounded topology perturbations, and extension to higher-dimensional joint queue-channel state models that capture time-varying fading alongside queue backlog.

## REFERENCES

- [1] J.-M. Lasry and P.-L. Lions, “Mean field games,” *Jpn. J. Math.*, vol. 2, no. 1, pp. 229–260, 2007.

- [2] M. Huang, R. P. Malhamé, and P. E. Caines, “Large population stochastic dynamic games: closed-loop McKean-Vlasov systems and the Nash certainty equivalence principle,” *Commun. Inf. Syst.*, vol. 6, no. 3, pp. 221–252, 2006.
- [3] Y. Kang, H. Wang, B. Kim, J. Xie, X.-P. Zhang, and Z. Han, “Time efficient offloading optimization in automotive multi-access edge computing networks using mean-field games,” *IEEE Trans. Veh. Technol.*, 2023.
- [4] D. Wang, W. Wang, Y. Kang, and Z. Han, “Distributed data offloading in ultra-dense LEO satellite networks: A Stackelberg mean-field game approach,” *IEEE J. Sel. Topics Signal Process.*, vol. 17, no. 1, pp. 112–127, Jan. 2023.
- [5] H. Zhang, H. Tang, Y. Hu, X. Wei, C. Wu, W. Ding, and X.-P. Zhang, “Heterogeneous mean-field multi-agent reinforcement learning for communication routing selection in SAGI-net,” in *Proc. IEEE VTC Fall*, 2022.
- [6] Y. Xu, X. Wu, Y. Tang, J. Shang, L. Zheng, and L. Zhao, “Joint resource allocation for V2X communications with multi-type mean-field reinforcement learning,” *IEEE Trans. Intell. Transp. Syst.*, vol. 26, no. 10, pp. 17462–17476, Oct. 2025.
- [7] B. Qiao, “Heterogeneous mean field games and local well-posedness,” arXiv:2511.19766v1, Nov. 2025.
- [8] R. M. Gray and D. L. Neuhoff, “Quantization,” *IEEE Trans. Inf. Theory*, vol. 44, no. 6, pp. 2325–2383, 1998.
- [9] P. E. Caines and M. Huang, “Graphon mean field games and the GMFG equations:  $\epsilon$ -Nash equilibria,” *SIAM J. Control Optim.*, vol. 59, no. 6, pp. 4512–4549, 2021.
- [10] R. Carmona, D. B. Cooney, C. V. Graves, and M. Laurière, “Stochastic graphon games: II. The linear-quadratic case,” *SIAM J. Control Optim.*, vol. 60, no. 4, pp. 2071–2100, 2022.
- [11] B. Guo, Z. Xiong, Z. Zhang, Q. Yang, B. Li, D. Niyato, M. Guizani, and Z. Han, “Lightweight semantic communication-compliant shortest path selection in large-scale LEO satellite networks,” *IEEE Trans. Mobile Comput.*, 2026.
- [12] R. Ding, F. Zhou, Q. Wu, K.-K. Wong, and N. Al-Dhahir, “Optimization-driven DRL for resource allocation under licensed and unlicensed UAV spectrum sharing networks against uncertain jamming,” *IEEE Trans. Mobile Comput.*, 2026.
- [13] A. Chambolle and T. Pock, “A first-order primal-dual algorithm for convex problems with applications to imaging,” *J. Math. Imaging Vis.*, vol. 40, no. 1, pp. 120–145, May 2011.
- [14] D. Wang, W. Wang, Y. Kang, and Z. Han, “Dynamic data offloading for massive users in ultra-dense LEO satellite networks based on Stackelberg mean field game,” in *Proc. IEEE INFOCOM Workshops*, London, UK, May 2022.
- [15] D. Wang, C. Huang, J. He, X. Chen, W. Wang, Z. Zhang, Z. Han, and M. Debbah, “Mean field game-based waveform precoding design for mobile crowd integrated sensing, communication, and computation systems,” arXiv:2309.02645v2, Feb. 2024.
- [16] Y. Kang, Y. Zhu, D. Wang, Z. Han, and T. Başar, “Joint server selection and handover design for satellite-based federated learning using mean-field evolutionary approach,” *IEEE Trans. Netw. Sci. Eng.*, vol. 11, no. 2, pp. 1655–1667, 2024, mar./Apr. 2024.
- [17] L.-H. Shen and J.-J. Huang, “Multi-functional RIS-enabled in SAGIN for IoT: A hybrid deep reinforcement learning approach with compressed twin-models,” arXiv:2507.16204v2, Oct. 2025.
- [18] W. Jiang, H. Han, M. He, and W. Gu, “When game theory meets satellite communication networks: A survey,” *Comput. Commun.*, vol. 217, pp. 208–229, 2024.
- [19] R. Carmona and F. Delarue, *Probabilistic Theory of Mean Field Games and Mean Field Type Control Theory*. New York, NY, USA: Springer, 2018.
- [20] N. Fournier and A. Guillin, “On the rate of convergence in Wasserstein distance of the empirical measure,” *Probab. Theory Related Fields*, vol. 162, pp. 707–738, 2015.
- [21] J. Weed and F. Bach, “Sharp asymptotic and finite-sample rates of convergence of empirical measures in Wasserstein distance,” *Bernoulli*, vol. 25, no. 4A, pp. 2620–2648, 2019.

## APPENDIX

## A. Proof of Lemma 1

We provide the complete proof of Lemma 1.

Under Assumption 1, for any two types  $k, k' \in [K]$ , let  $(X_0^{(k)}, X_0^{(k')})$  be an optimal coupling achieving  $W_2(\rho_0^{(k)}, \rho_0^{(k')})$ . We evolve both processes under the same Brownian motion  $W_t$  and their respective equilibrium controls  $\alpha^{*(k)}, \alpha^{*(k')}$ :

$$\begin{aligned} X_t^{(k)} &= X_0^{(k)} + \int_0^t b^{(k)}(X_s^{(k)}, \rho_s, \alpha_s^{*(k)}) ds + \sigma^{(k)} W_t, \quad (38) \\ X_t^{(k')} &= X_0^{(k')} + \int_0^t b^{(k')}(X_s^{(k')}, \rho_s, \alpha_s^{*(k')}) ds + \sigma^{(k')} W_t. \end{aligned} \quad (39)$$

Define  $\Delta_t := X_t^{(k)} - X_t^{(k')}$ . By the parameterized model (12), the drift difference satisfies:

$$\begin{aligned} \left| b^{(k)}(x, \rho, a) - b^{(k')}(x, \rho, a) \right| &= |\theta_k - \theta_{k'}| \cdot |b_1(x, \rho, a)| \\ &\leq |\theta_k - \theta_{k'}| \cdot L_b, \end{aligned} \quad (40)$$

where  $L_b$  is the uniform Lipschitz constant of  $b_1$ .

Applying the triangle inequality and Grönwall's lemma to  $\Delta_t$ :

$$\begin{aligned} \mathbb{E}|\Delta_t|^2 &\leq 2\mathbb{E}|X_0^{(k)} - X_0^{(k')}|^2 \cdot e^{2L_b t} + 2|\theta_k - \theta_{k'}|^2 L_b^2 \cdot \frac{e^{2L_b t} - 1}{2L_b} \\ &\leq e^{2L_b t} [\mathbb{E}|\Delta_0|^2 + |\theta_k - \theta_{k'}|^2 L_b^2 T^2], \end{aligned} \quad (41)$$

where in the last line we used  $\frac{e^{2L_b t} - 1}{2L_b} \leq T e^{2L_b T}$ .

Since  $(X_0^{(k)}, X_0^{(k')})$  is the optimal  $W_2$ -coupling,  $\mathbb{E}|\Delta_0|^2 = W_2^2(\rho_0^{(k)}, \rho_0^{(k')})$ . Thus:

$$\begin{aligned} W_2^2(\rho_t^{(k)}, \rho_t^{(k')}) &\leq \mathbb{E}|\Delta_t|^2 \\ &\leq e^{2L_b T} \left[ W_2^2(\rho_0^{(k)}, \rho_0^{(k')}) + |\theta_k - \theta_{k'}|^2 L_b^2 T^2 \right]. \end{aligned} \quad (42)$$

Taking the square root and using  $\sqrt{a+b} \leq \sqrt{a} + \sqrt{b}$ :

$$W_2(\rho_t^{(k)}, \rho_t^{(k')}) \leq e^{L_b T} \left[ W_2(\rho_0^{(k)}, \rho_0^{(k')}) + |\theta_k - \theta_{k'}| L_b T \right]. \quad (43)$$

Averaging over all pairs  $(k, k')$  with  $k \neq k'$ :

$$\begin{aligned} H_K(\rho_t) &= \frac{1}{K(K-1)} \sum_{k \neq k'} W_2(\rho_t^{(k)}, \rho_t^{(k')}) \\ &\leq e^{L_b T} \left[ H_K^{(0)} + L_b T \cdot \frac{1}{K(K-1)} \sum_{k \neq k'} |\theta_k - \theta_{k'}| \right] \\ &\leq e^{L_b T} \left[ H_K^{(0)} + L_b T \cdot \text{Var}(\theta)^{1/2} \cdot \sqrt{2} \right], \end{aligned} \quad (44)$$

where the last inequality follows from Cauchy-Schwarz:

$$\begin{aligned} \frac{1}{K(K-1)} \sum_{k \neq k'} |\theta_k - \theta_{k'}| &\leq \left( \frac{1}{K(K-1)} \sum_{k \neq k'} |\theta_k - \theta_{k'}|^2 \right)^{1/2} \\ &\leq \sqrt{2} \text{Var}(\theta)^{1/2}. \end{aligned} \quad (45)$$

Absorbing  $e^{L_b T}$  into the constants (bounded for  $T \leq \delta_0$ ) yields (13).  $\square$

## B. Proof of Lemma 2

Claims (i) and (ii) are special cases of the rates in [20] for  $d = 1$  and probability measures supported on a compact interval of length  $Q_{\max}$ . Claim (iii) is immediate from boundedness of  $\Omega$ .  $\square$

## C. Proof of Theorem 1 (Error Decomposition)

The proof combines a type-discretization bound with per-class empirical measure estimates as in Lemma 5.3 and Theorem 5.4 of [7].

**Step 1 (Discretization error).** For  $\theta \in [(k-1)/K, k/K)$  with representative  $\theta_k = (2k-1)/(2K)$ , Hölder regularity of  $b_1$  in  $\theta$  with constant  $[b_1]_\beta$  gives

$$|b(\theta, \cdot) - b(\theta_k, \cdot)| = |\theta - \theta_k|^\beta [b_1]_\beta \leq \left( \frac{1}{2K} \right)^\beta [b_1]_\beta. \quad (46)$$

Hence the discretization component of the error is  $O(K^{-\beta})$ ; we write it as  $C_1 K^{-\beta}$  with  $C_1$  absorbing  $[b_1]_\beta$  and related constants.

**Step 2 (Sample size error).** For balanced partitions,  $N_k \approx N/K$ . Let  $\hat{\rho}_n^{(k)} = \frac{1}{N_k} \sum_{i \in \mathcal{C}_k} \delta_{X_i}$ . Applying Lemma 2(ii) with  $n = N_k$  and matching the  $W_2$  distance used in the propagation-pf-chaos analysis of [7],

$$\mathbb{E} \left[ W_2 \left( \hat{\rho}_n^{(k)}, \rho^{(k)} \right) \right] \leq C_2^{\text{emp}} \cdot N_k^{-1/2} = C_2^{\text{emp}} \cdot \left( \frac{K}{N} \right)^{1/2}. \quad (47)$$

We set  $\alpha = 1/2$  (sharp for  $d = 1$ ) and absorb  $C_2^{\text{emp}}$  into the constant  $C_2$  in (17). Under Assumption 1, moments of  $\{\theta_k\}$  may be used to bound  $[b_1]_\beta$  and hence to relate  $C_1$  to  $\text{Var}(\theta)$  at the level of constants only. For unbalanced fleets, Lemma 2(ii) with  $n = n_{N,K}^{\min}$  yields (24).

**Combining both steps.**

Theorem 5.4 of [7] yields  $\varepsilon_{N,K} \leq C_1 K^{-\beta} + C_2 (K/N)^\alpha + C_3 \delta_{N,K}^{1/2}$ , i.e., (17).  $\square$

## D. Proof of Theorem 2

Consider the reduced error (18) from (17) with  $\delta_{N,K}$  negligible.

**Coercivity and existence.** As  $K \rightarrow 0^+$ , the term  $C_1 K^{-\beta}$  dominates and  $\mathcal{E}(N, K) \rightarrow +\infty$ ; as  $K \rightarrow +\infty$ , the term  $C_2 (K/N)^\alpha$  dominates and  $\mathcal{E}(N, K) \rightarrow +\infty$ . Since  $\mathcal{E}$  is continuous on  $(0, \infty)$ , a global minimizer exists.

**Uniqueness via the first derivative.** The derivative of (18) is

$$\frac{\partial \mathcal{E}}{\partial K} = -\beta C_1 K^{-\beta-1} + \frac{\alpha C_2}{N^\alpha} K^{\alpha-1}. \quad (48)$$

Define  $h(K) := \partial \mathcal{E} / \partial K$ . For small  $K$ , the negative power  $K^{-\beta-1}$  dominates, so  $h(K) < 0$ ; for large  $K$ , the term  $\propto K^{\alpha-1}$  is positive for typical  $(\alpha, \beta)$ , so  $h(K) > 0$  eventually. The equation  $h(K) = 0$  is equivalent to  $K^{\alpha+\beta} = (\beta C_1 / (\alpha C_2)) N^\alpha$ , which has a *unique* solution  $K^*(N) > 0$ , namely (19).

**Strict minimum.** Differentiating  $h(K)$  gives

$$h'(K) = \beta(\beta+1) C_1 K^{-\beta-2} + \alpha(\alpha-1) C_2 N^{-\alpha} K^{\alpha-2}. \quad (49)$$

At  $K^*$ , using  $h(K^*) = 0$  to write  $\beta C_1(K^*)^{-\beta-1} = (\alpha C_2/N^\alpha)(K^*)^{\alpha-1}$ ,

$$h'(K^*) = \beta(\beta+1)C_1(K^*)^{-\beta-2} + \alpha(\alpha-1)C_2N^{-\alpha}(K^*)^{\alpha-2} \quad (50)$$

$$= \frac{1}{K^*} \left[ (\beta+1)\beta C_1(K^*)^{-\beta-1} + (\alpha-1)\alpha C_2N^{-\alpha}(K^*)^{\alpha-1} \right] \quad (51)$$

$$= \frac{\alpha C_2}{K^*N^\alpha} (K^*)^{\alpha-1} [(\beta+1) + (\alpha-1)] \quad (52)$$

$$= \frac{\alpha C_2}{N^\alpha} (K^*)^{\alpha-2} (\alpha + \beta) > 0. \quad (53)$$

Thus  $h$  crosses zero strictly upward at  $K^*$ , so  $K^*$  is a strict local minimum; together with coercivity, it is the *unique* global minimizer. Substituting (19) into (18) yields (20).  $\square$

### E. Proof of Theorem 3 (LEO Topology Robustness)

Let  $\Phi_{\text{sat}}^{\tau_i} = \mu/B_{\text{sat}}^{\tau_i}$  denote the snapshot-wise backhaul surcharge on  $[i\Delta\tau, (i+1)\Delta\tau)$ . Consider the perturbed HJB value  $V_{\text{pert}}^{(k)}$  under  $\Phi + \Phi_{\text{sat}}$  and the static value  $V^{(k)}$  under  $\Phi$ . Define  $\delta V^{(k)} := V_{\text{pert}}^{(k)} - V^{(k)}$ .

**Step 1 (bounded forcing).** The perturbation enters the Hamiltonian as an additive forcing term of order  $\beta_2^{(k)} R^{(k)} \Phi_{\text{sat}}^{\tau(t)}$ . Under bounded rates and bounded snapshot surcharge, standard energy estimates for parabolic HJB equations imply

$$\sup_{t \in [0, T]} \|\delta V^{(k)}(\cdot, t)\|_{L^2(\Omega)} \leq C_k \|\Phi_{\text{sat}}\|_{L^2(0, T)}.$$

**Step 2 (snapshot-variation accumulation).** By assumption, adjacent snapshots satisfy  $|\Phi_{\text{sat}}^{\tau_i} - \Phi_{\text{sat}}^{\tau_{i+1}}| \leq \Delta_\Phi$ . Summing increments across  $M = \lceil T/\Delta\tau \rceil$  windows and applying Cauchy-Schwarz yields

$$\|\Phi_{\text{sat}}\|_{L^2(0, T)} \leq \bar{C} \Delta_\Phi \sqrt{T/\Delta\tau}.$$

Combining with Step 1 gives

$$\|\delta V^{(k)}\|_{L^\infty([0, T] \times \Omega)} \leq \tilde{C}_k \Delta_\Phi \sqrt{T/\Delta\tau}.$$

**Step 3 (impact on  $\varepsilon$ -Nash error).** The perturbed value gap induces an additive contribution in the finite-player  $\varepsilon$ -Nash bound, so

$$\varepsilon_{N, K}^{\text{LEO}} \leq \varepsilon_{N, K} + C_{\text{LEO}} \Delta_\Phi \sqrt{T/\Delta\tau},$$

with  $C_{\text{LEO}} := \max_k \tilde{C}_k$ , independent of  $N, K$ . This is (28).  $\square$

### F. Proof of Theorem 4 (Corrected Convergence Condition)

The proof extends the Chambolle-Pock convergence analysis [13] to the heterogeneous multi-type FPK system.

**Step 1: Homogeneous baseline ( $K = 1$ ).**

For a single vehicle type, the saddle-point problem (31) reduces to the standard G-prox PDHG of [3]. The augmented Lagrangian  $\mathcal{L}_\rho$  satisfies  $\|\nabla_\rho^2 \mathcal{L}_\rho\|_{\text{op}, \ell^2} \leq L_{\mathcal{L}}^2$  for some  $L_{\mathcal{L}} > 0$  depending on  $L, T, \|b_0\|$ . By Chambolle-Pock [13], convergence holds when  $\xi\varsigma < 1/L_{\mathcal{L}}^2$ , normalized to  $\xi\varsigma < 1$  after scaling  $(\xi, \varsigma)$  by  $L_A = L_{\mathcal{L}}$ .

**Step 2: Cross-type coupling (upper bound on cross-partial).**

With  $K$  types,  $\Gamma^{(k)}[\rho]$  is  $L$ -Lipschitz in  $\rho$  under Assumption 1. Applying the chain rule to the augmented Lagrangian and using dual regularity  $\nabla_q \phi^{(k)} \in L^\infty$  yields the pointwise estimate (37) stated in the main text; it is an upper bound, not an identity, so the step-size condition is only sufficient.

**Step 3: Operator norm bound via block aggregation.** Decompose the effective operator as  $\mathbf{A}_{\text{eff}} = \mathbf{A}_{\text{diag}} + \mathbf{A}_{\text{cross}}$ , where  $\mathbf{A}_{\text{diag}}$  is block-diagonal with spectral norm at most  $L_A$  and  $\mathbf{A}_{\text{cross}}$  captures cross-type coupling. By the triangle inequality and  $(a+b)^2 \leq 2a^2 + 2b^2$ ,

$$\|\mathbf{A}_{\text{eff}}\|_{\text{op}}^2 \leq 2L_A^2 + 2\|\mathbf{A}_{\text{cross}}\|_{\text{op}}^2. \quad (54)$$

Summing (37) over  $k \neq k'$  and bounding gradients by their supremum over iterations as in (35) produces a term of the form  $L_A^2 C_H H_K(\rho)$  up to an absolute constant factor; absorbing the factor 2 into  $C_H$  yields (34).

**Step 4: Sufficient convergence condition.**

Substituting (34) into (33) gives the raw sufficient condition before normalization. Rescaling  $(\xi, \varsigma)$  by  $L_A$  yields (36). When  $H_K(\rho) = 0$ , we recover  $\xi\varsigma < 1$  [3].  $\square$

### G. Complexity Analysis of Wasserstein Computation

In the 1D queue state space  $\Omega = [0, Q_{\text{max}}]$  with  $N_q$  discretization points, the Wasserstein-2 distance between two empirical distributions  $\rho^{(k)}$  and  $\rho^{(k')}$  reduces to the  $L^2$  distance between their quantile functions [7]:

$$\begin{aligned} W_2^2(\rho^{(k)}, \rho^{(k')}) &= \int_0^1 |F_k^{-1}(u) - F_{k'}^{-1}(u)|^2 du \\ &\approx \frac{1}{N_q} \sum_{i=1}^{N_q} |q_{(i)}^{(k)} - q_{(i)}^{(k')}|^2, \end{aligned} \quad (55)$$

where  $F_k^{-1}$  is the quantile function of  $\rho^{(k)}$  and  $q_{(i)}^{(k)}$  is the  $i$ -th order statistic.

**Sorting cost:** Computing  $N_q$  order statistics for each of  $K$  types requires  $O(KN_q \log N_q)$  operations.

**Distance computation:** After sorting, computing all  $K(K-1)/2$  pairwise distances requires  $O(K^2 N_q)$  operations.

**Total per-iteration cost:** The Wasserstein computation contributes  $O(K^2 N_q \log N_q)$  per iteration, which is dominated by the  $O(KN_q N_t)$  cost of the FPK/HJB updates (Proposition 3) since  $K \ll N_q$  in practice.

**Independence from vehicle count  $N$ :** Crucially, none of the above operations involve  $N$  directly. The mean field  $\rho^{(k)}$  is maintained as a probability distribution over the  $N_q$ -point state space grid, not as a sum of  $N_k$  empirical delta functions. This confirms that Algorithm 3 achieves computation time *independent of the number of vehicles*, analogous to the homogeneous G-prox PDHG of [3], [15].  $\square$

### H. Proof of Proposition 1

Direct substitution of  $C_1 = \bar{C}_1 H_\infty$  into (19) and simplification.  $\square$

*I. Proof of Corollary 2*

Since  $K^*$  is the unique global minimizer of the smooth function  $\mathcal{E}(N, \cdot)$  on  $(0, \infty)$ , Taylor expansion at  $K^*$  gives, for integer  $\hat{K}$  near  $K^*$ ,

$$\mathcal{E}(N, \hat{K}) - \mathcal{E}(N, K^*) \leq \frac{1}{2} |\hat{K} - K^*|^2 \cdot \mathcal{E}''(N, K^*) \leq \frac{1}{8} \mathcal{E}''(N, K^*). \quad (56)$$

Since  $|\hat{K} - K^*| \leq 1/2$  and  $\mathcal{E}''(N, K^*)$  scales polynomially in  $N$  while  $\mathcal{E}(N, K^*)$  decays as in (20), the relative gap is  $o(1)$  as  $N \rightarrow \infty$ .  $\square$

*J. Proof of Corollary 3*

The sample-size term is governed by the smallest class  $n_{N,K}^{\min} = \lambda_{\min} N$  (Proposition 2). Using  $N_k \geq \lambda_{\min} N$  for all  $k$ , the balanced surrogate  $C_2(K/N)^\alpha$  in (18) is replaced by  $C_2(K/(\lambda_{\min} N))^\alpha$ . Theorem 2 applied to this two-term functional yields (26).  $\square$

*K. Proof of Proposition 3*

Each iteration requires  $K$  parallel FPK/HJB updates of cost  $O(N_q N_t)$  each, plus  $K(K-1)/2$  Wasserstein distance computations. In 1D (queue length),  $W_2(\rho^{(k)}, \rho^{(k')})$  reduces to the  $L^2$  distance between quantile functions, computable in  $O(N_q \log N_q)$ . The total per-iteration cost is thus  $O(K^2 N_q N_t)$ , independent of  $N$ .  $\square$